Universiteit van Amsterdam

Vrije Universiteit Amsterdam

Master Thesis

Study of charm hadronisation mechanisms from small to large collision systems with the ALICE experiment

Yonne Lourens

14076128

First supervisor: Dr. Panos Christakoglou
Daily supervisor: Dr. Marco Giacalone
Second reader: Dr. Alessandro Grelli

July 17, 2024

Submitted in partial fulfillment of the requirements for the joint UvA-VU degree of Master of Science in Physics & Astronomy

Acknowledgements

I want to take the time here to sincerely thank, first of all, my daily supervisor Marco. During the past year and my summer project at CERN, you were an excellent and inspiring supervisor, who also genuinely cared about his students. I want to thank you for all the invaluable support and opportunities you gave me. I wish you all the best in your future endeavors at CERN. I also want to thank my first supervisor Panos who helped me tailor this project within the ALICE collaboration at Nikhef. I want to thank you for your insightful advice and patience throughout the project. I appreciate the space you gave me to try different things, for example, lots of teaching, which was an invaluable experience. I wish you the best in Maastricht. I would also like to thank my second reader Alessandro. Moreover, I want to thank my family and friends for their support, fun holidays and distractions. Finally, I would thank the most important of all, Lisa. You have been watching my physics and maths journey from the sidelines for the past 6 years. Years I would not have wanted to spend without you. I am extremely grateful that you joined me in Geneva. It was a great adventure, and I am sure we will keep making new ones in the future.

Abstract

In this thesis, the production of heavy-flavour hadrons containing a charm quark in pp, p–Pb and Pb–Pb collisions will be discussed. Various hadronisation models that are implemented in commonly used event generators, such as PYTHIA8 (including QCD-CR models), HERWIG7 (including baryonic clustering models) and EPOS4, are inspected. With this background, Monte-Carlo generated data are compared with ALICE experimental results. The RIVET framework is mainly used for the study, allowing us to perform a systematic, easy-to-implement and standardised comparison between simulated data and measurements. A selection of comparisons between simulated data and recent measurements on meson-to-meson, baryon-to-meson and baryon-to-baryon production ratios is presented.

The default PYTHIA8 Monash tune and HERWIG7, both tuned on measurements in $e^{+}e^{-}$ collisions, significantly underestimate charmed baryons production in pp collisions. On the other hand, both PYTHIA8 QCD-CR Mode 2 and Mode 0 describe Λ_c^+ production well due to the formation of string junctions and string fragmentation mechanisms. Both tunes overestimate the production of $\Sigma_c(2455)$ baryons significantly. Furthermore, they do not adequately describe ratios between pseudoscalar and vector D-mesons. For this reason, a parameterization-based tuning is performed on the PYTHIA8 QCD-CR Mode 2 tune, using the `Apprentice` framework, for the `StringFlav:mesonCvector` and `StringFlav:probQQ1toQQ0join` flavour selection parameters. The minimization of the goodness-of-fit measure was performed with the Truncated Newton method and a Bayesian inference technique. The resulting tuned parameters are given in bold in Tab. 2. The predictions from PYTHIA8 CR Mode 2 with the tuned parameters are significantly improved for the D-meson ratios and Σ_c spectra, now describing the measurements within uncertainties. Due to the absence of strangeness enhancement mechanisms in QCD-CR tunes, the production of Ξ_c-baryons is still largely underestimated. The production of Ξ_c-baryons is better described by EPOS4 including a full core-corona procedure and hadronic rescattering mechanisms. Similarly, ratios between prompt D-mesons including strangeness are best described by EPOS4.

The production of charmed hadrons in heavy-ion collisions is studied with PYTHIA8 using Angantyr, without assuming the creation of a Quark-Gluon Plasma (QGP). We observe an enhancement of baryon production in highly string-dense environments by implementing beyond-leading color effects in the hadronization of individual sub-collisions.

Contents

1 Introduction

In this thesis, a study on open heavy-flavour production in high-energy proton-proton (pp), proton-lead (p–Pb), and lead-lead (Pb–Pb) is presented. The production of heavy-flavour hadrons can be used as an excellent probe to study the Quark Gluon Plasma (QGP), a deconfined state of matter created at very high energy densities and temperatures achievable with ultra-relativistic heavy-ion collisions, which is predicted by the strong interaction theory [1]. To study the QGP production, it is important to take into account pp and p–Pb collision measurements, so that any production mechanism difference can be discovered. Besides, studying pp collisions provides new insight into perturbative QCD (pQCD) calculations, while p–Pb collisions are a valid tool to inspect Cold Nuclear Matter effects. In this first chapter, a general introduction to the physics studied in the ALICE experiment is provided.

1.1 Quantum Chromo-Dynamics

Quantum Chromo-Dynamics (QCD) is the quantum field theory that describes the strong interaction between quarks and gluons. Similar to the electric charge in Quantum Electrodynamics (QED), the conserved colour charge is introduced in QCD for strong interactions. This charge can take on three different values for quarks, which are commonly called red (R), blue (B) and green (G). Logically, anti-quarks have corresponding anti-colour quantum numbers. To be more specific, the quarks are assigned to a triplet of an SU(3) colour group. The physical gluons that mediate the QCD force between the colour charges come in eight different colour combinations, so they belong to an SU(3) octet. The remaining combination, the SU(3) singlet, does not carry colour charge and cannot mediate the QCD force between the colour charges [2]. QCD is a non-Abelian gauge theory based on these colour-charged particles, relying on local SU(3) group transformations. We can describe these transformations mathematically as [22]:

$$\psi_k \to \psi'_j = \exp\,[ig_s\alpha_a T^a_{jk}]\psi^k, \tag{1.1}$$

where T^a_{jk} are the generators of the SU(3) transformation (represented by the Gell-Mann matrices), g_s the coupling strength and α_a are the corresponding complex fields. The QCD Lagrangian must be invariant under the transformations from Eq. 1.1 (by gauge invariance). Therefore, the QCD Lagrangian is given by [3]

$$\mathcal{L}_{\text{QCD}} = \bar{\psi}(i\gamma^\mu(\partial_\mu - ig_s A^a_\mu T_a) - m)\psi - \frac{1}{4}F^a_{\mu\nu}F^{\mu\nu}_a, \tag{1.2}$$

where ψ is the Dirac spinor of the quark field of a quark with mass m, γ^μ are the Dirac matrices, A^a_μ is the gluon field, and $F^a_{\mu\nu}$ is a fully gluonic tensor commonly expressed as

$$F^a_{\nu\mu} = \partial_\mu A^a_\nu - \partial_\nu A^a_\mu - g_s f^a_{bc} A^b_\mu A^c_\nu. \tag{1.3}$$

The complex fields α_a in the transformation Eq. 1.1 are absent in Eq. 1.2 due to canceling with the corresponding term in the covariant derivative acting on the quark and gluon fields, resulting in a Lagrangian that remains unchanged. In Eq. 1.3 g_s is the coupling constant, which is expressed as $\alpha_s = g^2/4\pi$ ($\hbar = c = 1$), and f^a_{bc} are the structure constants of SU(3).

The first two terms in the Lagrangian Eq. 1.2 are similar to the QED Lagrangian, as they describe vertices with two quarks and one gluon. The last term in Eq. 1.2 describes three- and four interaction vertices between gluons, more specifically the term $g_s f^a_{bc} A^b_\mu A^c_\nu$ produces self-interaction among gluons. This term can also produce the anti-screening phenomenon in colour interactions. The fact that the carrier can self-interact is not seen in QED and is a unique feature in QCD.

In nature, neither gluons nor quarks are observed as free particles. The particles that are however detected, are colour-neutral (colour-singlet) combinations of quarks and gluons, called hadrons. This phenomenon is called colour confinement, or simply confinement. The bounding force that holds the quarks together can be approximated at large distances by a potential increasing linearly with the distance between the partons. Due to this increase, it becomes energetically more favorable to create new quark-antiquark pairs when the distance between the initial pair becomes larger, see Fig. 1.

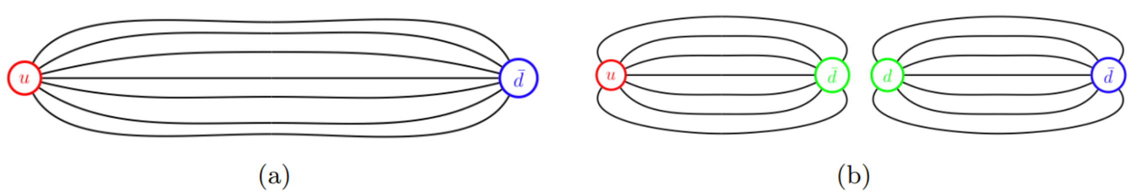

Figure 1: (a) Bounded quark and anti-quark pair in a mesons. Gluon *exchange* is represented by flux tubes as field lines. (b) Separation of a quark-antiquark pair. The energy of the gluon field increases, until the breaking of flux tubes becomes energetically favorable. Figure is taken from [19].

The potential V_{QCD} between a quark-antiquark pair is often expressed as [4]

$$V_{\text{QCD}}(r) = -\frac{4}{3}\frac{\alpha_s(r)}{r} + \sigma \cdot r, \tag{1.4}$$

where r is the distance between the quark and anti-quark, α_s is the QCD coupling constant and σ is the string tension.
For a given squared momentum transfer Q^2 the coupling constant can be calculated with [24]

$$\alpha_s = \frac{g_s^2}{4\pi} = \frac{\alpha_s(M^2)}{1 + \alpha_s(M^2)\frac{33-2n_f}{12\pi}\ln\frac{Q^2}{M^2}}, \tag{1.5}$$

where n_f is the number of flavours and M the renormalisation mass scale [4]. One can derive from Eq. 1.5 that α_s becomes small when Q^2 increases, and thus in high-energy processes (i.e. on short distances) partons can behave similarly to free particles, which is commonly called asymptotic freedom. However, for lower Q^2 values, α_s increases, indicating the confinement of partons. Several experiments validate the *running* behavior of the coupling constant relative to squared momentum transfer Q^2, as illustrated in Fig. 2.

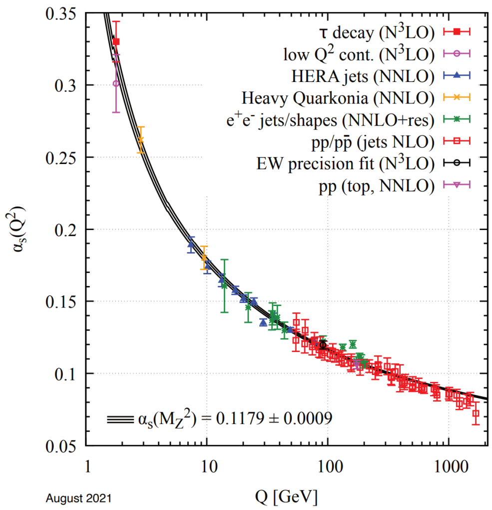

Figure 2: The running coupling constant α_s as a function of Q^2. Figure is taken from [5].

In the regime $Q^2 > 1$ GeV$^2/c^2$, perturbative QCD calculations (such as cross sections estimations) can be performed since α_s is small, see Fig. 2. However, this approach can not be applied to even lower momenta, due to the divergence of the coupling constant. In such instances, the QCD Lagrangian can be assessed through lattice QCD calculations utilising a discrete space-time grid [6].

1.2 Probing the Quark Gluon Plasma

The description of collisions between two ultra-relativistic heavy nuclei is very complex. In general, there are commonly a few phases defined in heavy-ion collisions which are described by their respective space-time evolution.

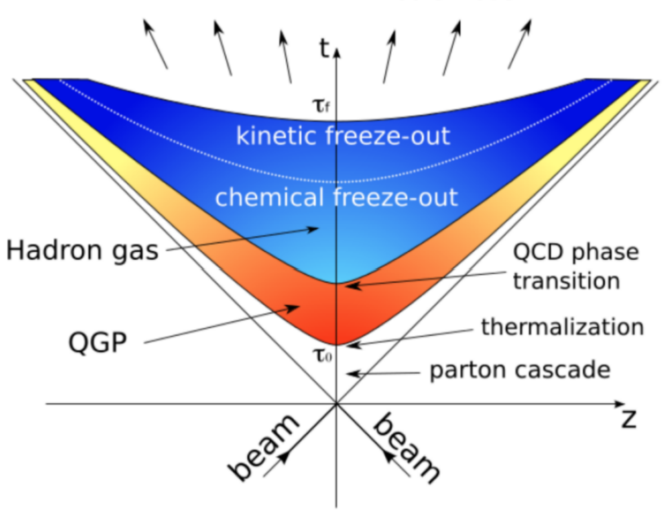

Figure 3: Space-time evolution of heavy-ion collisions with various stages illustrated. Figure is taken from [7].

As illustrated in Fig. 3 we commonly define the following phases [25]:

1. Initial stage: the collisions between the two heavy-ions happen in a relatively short time, ~ 0.3 fm/c. The initial state describes the position of the nuclei inside the colliding nuclei that fluctuate from one collision to the other. This results in different energy density profiles on every event which can have direct implications to final state observables.

2. Pre-equilibrium (parton cascade): Hard partons (e.g. heavy quarks) are produced during this phase by multiple parton interactions. This process lasts $\tau \simeq 0.3 - 2$ fm/c.

3. QGP formation (thermalisation): if the system reaches the critical temperature it becomes a deconfined phase and the QGP is formed. The whole system will expand simultaneously, so the temperature in the system starts to decrease.

4. Hadronisation: the gluons and quarks are no longer deconfined, and they start to hadronize into hadrons. The QGP becomes a hadron gas. This phase lasts about $\tau \simeq 6 - 10$ fm/c.

5. Freeze-out: for $\tau \gtrsim 10$ fm/c, the system will evolve into a freeze-out stage. At first, the inelastic interactions in the system will stop, meaning that the particle abundance is fixed. This is also known as the chemical freeze-out. Secondly, the elastic interaction will stop, and thus the momentum spectra of the produced particles are fixed (kinetic freeze-out).

The freeze-out of the QGP is reached at about 10 fm/c after the initial collision, and thus directly observing the QGP is not possible. However, some of the information about the system's evolution is preserved in the final-state particles, which are commonly called probes. In this thesis, we will only deal with hard probes, since heavy quarks (like the charm quark) are produced in hard scatterings of partons with a large transverse momentum (i.e. $1/Q \ll 1$ fm/c) before the formation of the QGP. For this reason, the hard partons (and their respective parton showers) experience the evolution of the entire system. Other examples of hard probes are jets, particles with high transverse momenta (p_T) and quarkonia. Relevant to this thesis are the hadrons containing heavy quarks.

In heavy-ion collisions, heavy-quarks that will pass through the QGP will interact with the medium and lose part of their energy through collisional and radiative energy loss mechanisms, see Sec. 2.1 for more detail. This suppression can be expressed quantitatively as the so-called nuclear modification factor

$$R_\mathrm{AA} = \frac{\mathrm{d}^2 N_\mathrm{AA}/\mathrm{d}p_\mathrm{T}\mathrm{d}y}{\langle T_\mathrm{AA}\rangle \cdot \mathrm{d}^2\sigma_\mathrm{pp}/\mathrm{d}p_\mathrm{T}\mathrm{d}y} = \frac{\mathrm{d}^2 N_\mathrm{AA}/\mathrm{d}p_\mathrm{T}\mathrm{d}y}{\langle N_\mathrm{coll}\rangle \cdot \mathrm{d}^2 N_\mathrm{pp}/\mathrm{d}p_\mathrm{T}\mathrm{d}y}, \tag{1.6}$$

where $\langle T_\mathrm{AA}\rangle$ is the average nuclear overlap function, defined as the average number of nucleon-nucleon collisions $\langle N_\mathrm{coll}\rangle$ divided by the inelastic proton-proton cross section. The number of binary nucleon-nucleon collisions can be estimated with the Glauber Model [8]. Furthermore, $\mathrm{d}N_\mathrm{AA}$ is the particle yield in heavy-ion collisions and $\mathrm{d}\sigma_\mathrm{pp}/\mathrm{d}p_\mathrm{T}$ the differential cross-section in pp collisions which is used as a reference. A deviation from unity of R_AA implies differences of the p_T distribution of the produced particles because of the interactions with the QGP medium or due to other nuclear processes, which are discussed in Sec. 1.3. These last effects can be studied by analysing the nuclear modification factor in R_{pPb} in p–Pb collisions. An example of R_{AA} measured in Pb–Pb collisions at $\sqrt{s_{NN}} = 5.02$ TeV with ALICE is shown in Fig. 4a for central collisions (0–10%). A significant energy loss of higher p_T charm quarks is observed by interacting with the QGP medium.

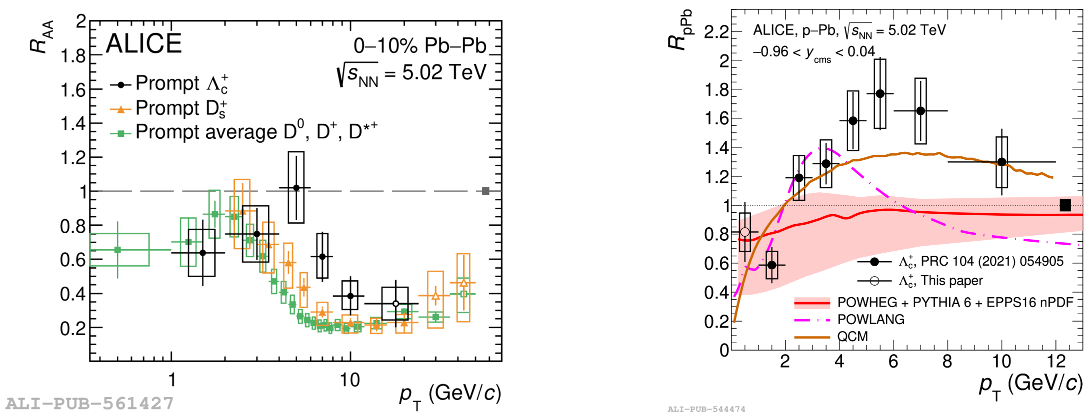

(a) (b)

Figure 4: (a) Nuclear modification factor R_{AA} of prompt Λ_c^+ baryons in central (0–10%) Pb–Pb collisions, compared with R_{AA} of D-mesons. (b) Nuclear modification factor R_{pPb} of prompt Λ_c^+ baryons in p–Pb collisions compared with models. Both R_{AA} and R_{pPb} are measured at $\sqrt{s_{NN}} = 5.02$ TeV and as a function of p_T. Figures are taken from [44] and [39] respectively.

1.3 Cold Nuclear Matter Effects

As a result of the large variation in the strong coupling constant, the properties of nuclear matter can be vastly different. The first experimental evidence of cold nuclear effects, such as gluon saturation and nuclear shadowing, was discussed in the early 80's [45]. It was found that the parton distribution functions (PDFs) of nucleons in a nuclear environment are different from that of isolated nucleons. In Eq. 2.2 we will see that the PDFs describe the parton density carrying a momentum fraction x (Bjorken-x) of the total momentum carried by the nucleon to which the parton belongs. We can quantify this difference by studying the ratio between nuclear PDFs (nPDFs) $f_i^A(x, Q^2)$ and isolated PDFs $f_i^N(x, Q^2)$ as a function of Bjorken-x as:

$$R_i^A(x, Q^2) = \frac{f_i^A(x, Q^2)}{f_i^N(x, Q^2)}, \tag{1.7}$$

where i is the index of the parton, such as the valence quarks, sea quarks, or the gluons. Fig. 5 shows the calculation of $R_i^A(x, Q^2)$ as a function of x, under the EPPS16 parametrization [46]. As one can see, according to this model, different cold nuclear effects appear in different regions of Bjorken-x. At low x (< 0.1), the number of produced gluons rapidly increases. This will result in more gluon self-interaction, and then the gluons can scatter off each other thus producing destructive interference. Therefore, the incoming nucleon will suffer a lower flux of gluons compared to a proton. This phenomenon is also called shadowing. As Bjorken-x increases, the shadowing effect diminishes, and the region for $0.1 < x < 0.3$ is called the anti-shadowing region. Besides the shadow effects, cold nuclear effects can also broaden the momentum distribution of partons, which is called k_T-broadening or Cronin enhancement [47]. The main source of this enhancement comes from the partonic multiple re-scatterings in the initial state. It consists of an enhancement of hadron production in p–A compared to pp collisions (when scaled by the number of binary nucleon-nucleon collisions $\langle N_{\rm coll}\rangle$).

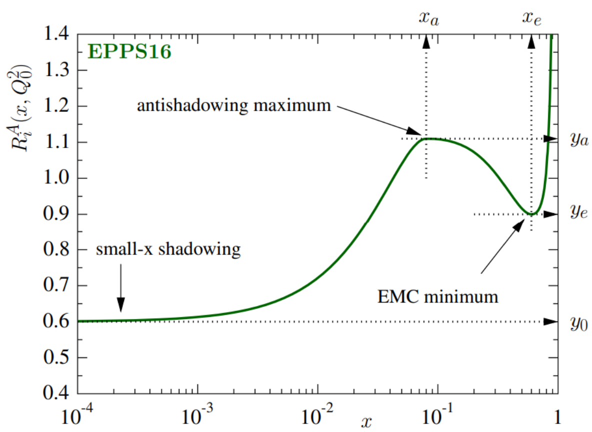

Figure 5: EPPS16 parameterisation of $R_i^{\rm A}(x, Q^2)$ as a function of Bjorken-x. Figure is taken from [46].

Similar to the definition of nuclear modification factor $R_{\rm AA}$ in Eq. 1.6, we can define a observable $R_{\rm pPb}$ in p–Pb collisions

$$R_{\rm pPb} = \frac{{\rm d}^2 N_{\rm pPb}/{\rm d}p_{\rm T}{\rm d}y}{\langle T_{\rm pPb}\rangle \cdot {\rm d}^2\sigma_{\rm pp}/{\rm d}p_{\rm T}{\rm d}y} = \frac{{\rm d}^2 N_{\rm pPb}/{\rm d}p_{\rm T}{\rm d}y}{\langle N_{\rm coll}\rangle \cdot {\rm d}^2 N_{\rm pp}/{\rm d}p_{\rm T}{\rm d}y}, \tag{1.8}$$

where $N_{\rm pPb}$ is the particle yield in p–Pb collisions, ${\rm d}\sigma_{\rm pp}$ is the inelastic cross section in pp collisions, $\langle T_{\rm pPb}\rangle$ is the nuclear overlap function which can be defined as $\langle T_{\rm pPb}\rangle = \langle N_{\rm coll}\rangle/\sigma_{\rm pp}$, where $\langle N_{\rm coll}\rangle$ can be determined by the Glauber model [8]. In Fig. 4b, the $R_{\rm pPb}$ of prompt $\Lambda_{\rm c}^+$ at $\sqrt{s_{\rm NN}} = 5.02$ TeV is shown as a function of $p_{\rm T}$ and is compared to model predictions. The $R_{\rm pPb}$ shows a clear maximum in the intermediate $p_{\rm T}$ range ($4 < p_{\rm T} < 8$ GeV/c), which can be explained by Cronin enhancement. In the high $p_{\rm T}$ region, i.e. $p_{\rm T} > 10$ GeV/c, the $R_{\rm pPb}$ is consistent with unity.

2 Open heavy-flavour physics

2.1 Open heavy-flavour production

Heavy quarks (Q), like charm (c) and bottom quarks (b), are produced in hard scattering processes during the early stages of the collisions. The quarks are considered heavy because their masses ($m_b \approx 4.2$ GeV and $m_c \approx 1.3$ GeV [21]) are large compared to the temperature of the QGP [20]. As a consequence of the flavour conservation law in the strong interaction, these quarks are solely produced in $b\bar{b}$ and $c\bar{c}$ pairs, which can later hadronise in charmonia/bottomonia states or into open heavy-flavour hadrons, which are hadrons with a non-zero charm or beauty number, like for example the Λ_c^+ baryon (udc) [24]. $Q\bar{Q}$ pairs at leading order (LO) ($\mathcal{O}(\alpha_s^2)$) are either produced by gluon fusion ($gg \rightarrow Q\bar{Q}$) or quark-antiquark annihilation ($q\bar{q} \rightarrow Q\bar{Q}$). At next-to-leading order (NLO), corresponding to $\mathcal{O}(\alpha_s^3)$, gluon-splitting ($gg \rightarrow Q\bar{Q}g$) and flavour-excitation processes ($gq \rightarrow Q\bar{Q}q$) also contribute to the production. These scatterings require a minimum momentum transfer of $Q^2 \gtrsim 4m_{c,b}^2$, meaning that the production is essentially restricted to hard scattering processes in the initial stages of the collisions [26].

Since these initial hard scattering processes require a large momentum transfer Q^2, the value of the coupling constant α_s is lower than unity, meaning that heavy quark-antiquark pair production can be used to test perturbative QCD (pQCD) calculations down to low transverse momenta p_{T} [23]. To calculate the differential production cross-section down to low p_{T} of open heavy-flavour hadrons in pp collisions, i.e. $\sigma_{pp \rightarrow H_Q + X}$, one can use pQCD calculations using the (collinear) factorization approach by combining different terms in the equation [24]:

$$\mathrm{d}\sigma_{pp \rightarrow H_Q + X} = \sum_{i,j=q,\bar{q},g} f_1(x_i; \mu_f^2) \cdot f_2(x_j; \mu_f^2) \otimes \mathrm{d}\tilde{\sigma}_{ij \rightarrow Q\bar{Q}}(x_i; x_j; \mu_f^2; \mu_R^2) \otimes D_Q^{H_Q}(z). \tag{2.1}$$

In summary, the first term describes the product of two parton distribution functions (PDFs) f_1 and f_2 of the initial colliding protons (labeled respectively 1 and 2), which in turn describe the probability of locating a parton (i, j) inside the respective proton while carrying a momentum fraction $x_{i,j}$ of the total momentum of the proton. The second term describes the direct production cross-section of a heavy quark-antiquark pair via parton interaction, i.e. hard scattering; the third term is the fragmentation function (FF) part, describing the probability of a heavy quark Q hadronising into the hadron H_Q with momentum $p_H = zp_Q$. As seen in Eq. 2.1, the first two terms depend on an arbitrary scale μ_f, called the factorisation scale. The partonic cross-section is also dependent on the renormalisation scale μ_R, at which the strong coupling constant α_s is calculated, meaning that $\mathrm{d}\tilde{\sigma}_{ij \rightarrow Q\bar{Q}}$ can be estimated with pQCD calculations. Usually, the scales μ_f and μ_R are determined at the hard scale $\mu_f \sim \mu_R \sim \sqrt{m_{\mathrm{Q}}^2 + p_{\mathrm{T,Q}}^2}$, and are varied around this value to determine the theoretical uncertainties. Both the PDFs and FFs describe non-perturbative QCD processes and are therefore typically parametrised from measurements. Usually, the FFs are taken from $\mathrm{e}^+\mathrm{e}^-$ collision measurements by assuming universality among all the different collision systems. However, as we will see, this assumption is questioned by recent measurements.

While writing this thesis, the most accurate pQCD computations utilise the FONLL [29] and GM-VFNS [30] frameworks. Fig. 6a shows, for example, ALICE measurements on the differential cross section of prompt D^0 in pp collisions at $\sqrt{s} = 5.02$ TeV compared with the prediction of GM-VFNS.

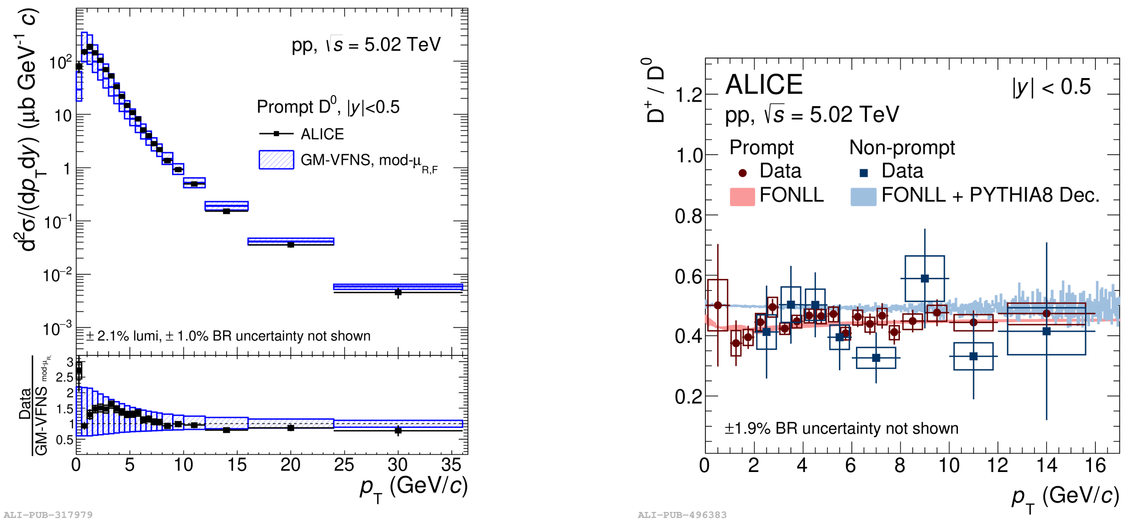

(a) (b)

Figure 6: Production cross section D^0 compared to theoretical predictions from GM-VFNS (left), and D^+/D^0 production ratios compared to FONNL predictions, both as a function of p_T. Figures are taken from [31] and [33] respectively.

In Fig. 6a it is clear that the differential cross-section of prompt[1] D^0 mesons as a function of p_T is compatible with GM-VFNS calculations, within their theoretical uncertainties. These uncertainties are larger than the experimental ones, which as already mentioned, come from the arbitrary choice of scales in the pQCD calculations. In Fig. 6b, in the case of the production ratios between different hadron species (also true for ratios between different rapidity regions and energies), these theoretical uncertainties are smaller compared to the experimental ones, making the theoretical prediction more sensitive to the PDFs and FFs. From Fig. 6 it can be inferred that pQCD calculations describe well the measurements for both prompt and non-prompt meson production.

[1] *Prompt* indicates the direct production of a specific hadron containing charm from the hard scattering, *Non-prompt* production refers to the charm production from beauty decay.

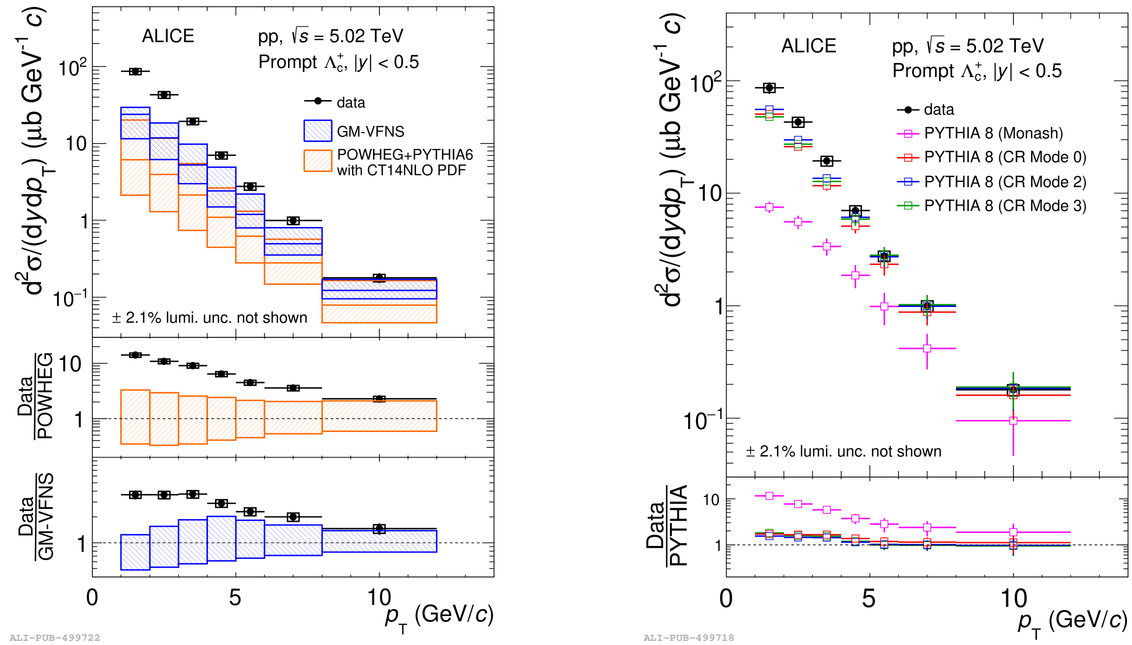

(a) (b)

Figure 7: Measurements of the p_{T}-differential production cross section for prompt Λ_c^+ in pp collisions at $\sqrt{s} = 5.02$ TeV with the ALICE experiment compared to (a) theoretical predictions, and (b) Monte Carlo models. Figures are taken from [43].

All previously made statements are valid for heavy-flavour mesons, like the D^0. However, when we compare theoretical predictions with heavy-flavour baryon production one can observe, for example as presented in Fig. 7a, that the same theoretical predictions significantly underestimate measurements of heavy-flavour baryon production. Furthermore, this behaviour is also clearly visible in Monte Carlo expectations, as seen in Fig. 7b, where PYTHIA8 (including different tunes), underestimates the baryon production.

In AA collisions additional mechanisms affect the production of charmed hadrons. As mentioned, heavy quarks are generated in the initial stages of the collision, before the formation of the QGP. This implies that heavy quarks traverse the QGP and can interact with the medium. They can therefore lose energy through inelastic (gluon radiation) and elastic (collisional) processes. By using the same notation and factorisation method as in Eq. 2.1, the production of heavy-flavour hadrons in AA collisions can be calculated as follows [25]:

$$\begin{aligned} \mathrm{d}\sigma_{AA\to H_Q+X} = A\cdot A \sum_{i,j=q,\bar{q},g} & f_1^N(x_i;\mu_f^2)\cdot f_2^N(x_j;\mu_f^2) \\ & \otimes \mathrm{d}\tilde{\sigma}_{ij\to Q\bar{Q}}(x_i;x_j;\mu_f^2;\mu_R^2) \\ & \otimes R_N^{QGP}(E,m_Q,T,\alpha,L,\dots)\otimes D_Q^{H_Q,N}(z). \end{aligned} \tag{2.2}$$

Compared to Eq. 2.1, the PDFs $f_1(x_i;\mu_f^2)$ and $f_2(x_j;\mu_f^2)$, and the fragmentation function $D_Q^{H_Q}$, are replaced by a modified PDF $f_1^N(x_i;\mu_f^2)$ and $D_Q^{H_Q,N}$, since we care about nuclear environment effects. Additionally, we introduce a new term R_N^{QGP} which represents the modification of the momentum of the heavy-quark due to energy loss in the QGP medium. This term shows that this energy loss (ΔE) is dependent on particle properties such as energy E, quark mass m_Q, as well as properties of the medium such as thickness L, temperature T and coupling of particle-medium interaction α [25]. In principle, the total loss of energy can be expressed as

$$\Delta E = \Delta E_{\text{coll}} + \Delta E_{\text{rad}}, \tag{2.3}$$

where ΔE_{rad} and ΔE_{coll} describe the radiative energy loss and the collisional energy loss respectively. At low transverse momentum, this energy loss is dominated by collisional energy loss via elastic scatterings with the constituents of the medium. At higher p_{T}, the mass of the quark becomes negligible (i.e. $m_Q \ll p_{\text{T}}$) and the quarks will behave similarly to light particles, which primarily lose energy via gluon radiation (radiative energy loss). Fig. 8 shows the comparison of collisional and radiative energy loss for charm quarks as a function of their energy, which is obtained within a theoretical framework of hydrodynamics coupled to a Langevin equation [48]. A more detailed discussion will be present in Sec. 3.3, where we will discuss the in-medium energy loss mechanisms implemented in EPOS4.

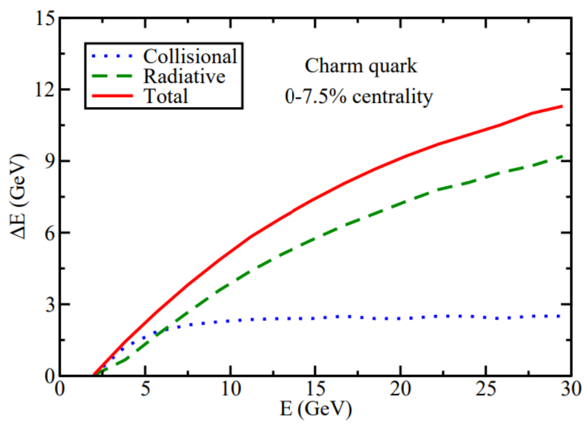

Figure 8: Comparison of collisional and radiative energy loss for charm quark in the QGP medium as a function of quark energy. Figure is taken from [48].

2.2 Heavy-flavour hadronisation

To describe heavy-flavour hadronisation it is typical to consider two types of mechanisms, namely hadronisation via recombination (also known as coalescence) and fragmentation. Due to the presence of the dense and hot QGP, the hadronisation process could be different in heavy-ion collisions, as described in Eq. 2.2. For example, heavy quarks can recombine with lighter quarks present in the medium and thus generate final state hadrons with a larger momentum than one of the initial partons. In this particular case, the recombination mixes with the fragmentation mechanism, where the latter is expected to dominate at high transverse momentum p_{T}, and the former is more related to the production of charmed hadrons at low p_{T} [49].

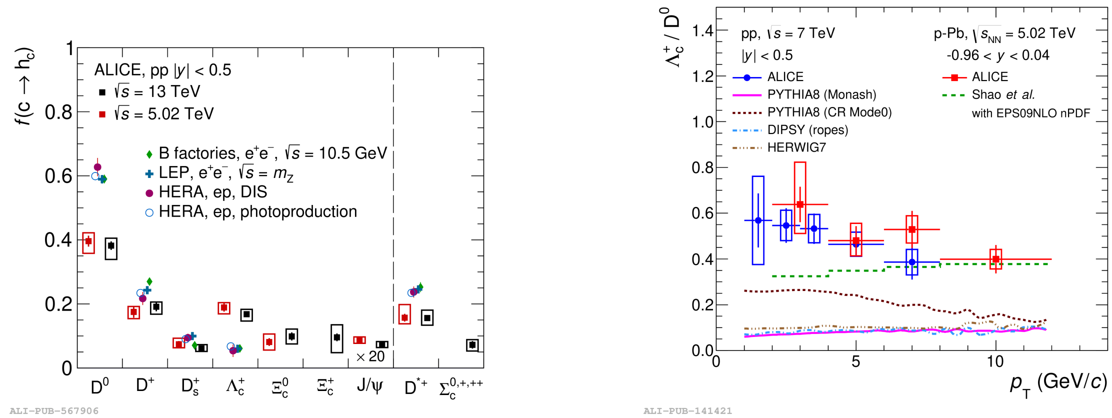

(a) (b)

Figure 9: (a) Charm fragmentation fractions $f(c \to h_c)$ for different hadron species as measured by different experiments in e^+e^-, ep and pp collisions. (b) Measurement of the Λ_c^+/D^0 production ratio as a function of transverse momentum p_T by the ALICE experiment compared to different Monte Carlo models. Figures are taken respectively from [37] and [42].

As already mentioned, the charm fragmentation function includes the probability of a charm quark c fragmenting into a charmed hadron h_c with lower momentum, known as the fragmentation fraction. Fig. 9a shows fragmentation fractions for charm hadrons measured by different experiments in multiple collision systems. It is clear that the measurements in a clean environment without nuclear effects, like in ep and e^+e^- collisions, are compatible within experimental uncertainties. However, as seen in Fig. 9a, different results are observed in hadronic collision systems like pp, suggesting the non-universality of fragmentation fractions. For example, the fragmentation fractions of D^0 and Λ_c^+ differ significantly. This difference led to the development of various theoretical models, that tried to reproduce these measurements.

In Fig. 9b the measured Λ_c^+/D^0 baryon-to-meson ratio as a function of p_T is compared to different Monte Carlo models. This observable is useful since it is sensitive to hadronisation mechanisms, and it can be used to probe different collision systems. Fig. 9b shows also that models tuned on e^+e^- and ep measurements, like PYTHIA8 Monash and HERWIG7, significantly underestimate the magnitude and do not show the same decreasing trend of the ratio measured in pp and p–Pb collisions. For the integrated-p_T Λ_c^+/D^0 measurement, average LEP measurements in e^+e^- collisions demonstrated a ratio of $0.113 \pm 0.013 \pm 0.006$ [34], which is significantly lower than the results for p–Pb and pp collisions at $\sqrt{s_{NN}} = 5.02$ TeV obtained by ALICE, which are $0.42 \pm 0.03 \pm 0.06$ and $0.51 \pm 0.04 \pm 0.04$ respectively [38]. We can also observe that the production yield ratio is of similar magnitude within experimental uncertainties for pp and p–Pb collisions [43].

In Pb–Pb collisions, the baryon-to-meson ratio Λ_c^+/D^0 is measured in Fig. 10a in the centrality classes 0-10% (central) and 30-50% (mid-central) at $\sqrt{s_{NN}} = 5.02$ TeV with ALICE. When we compare them to the pp measurements at the same energy, the magnitude of the baryon-to-meson ratio of Λ_c^+ and D^0 in Pb–Pb collisions is significantly larger. Also, the ratio is increasing from mid-central to central collisions, see Fig. 10a. The production cross-section of prompt Λ_c^+ is shown in Fig. 10b. One can see that the measurement of the cross-section in Pb–Pb is compatible with the scaled pp reference within uncertainties for low p_T. This implies that the nuclear modification factor (R_{AA}) is consistent with unity for $p_T < 6$ GeV/c, while the cross-section in Pb–Pb gets suppressed for larger p_T, which implies an energy loss of the charm quarks in the QGP.

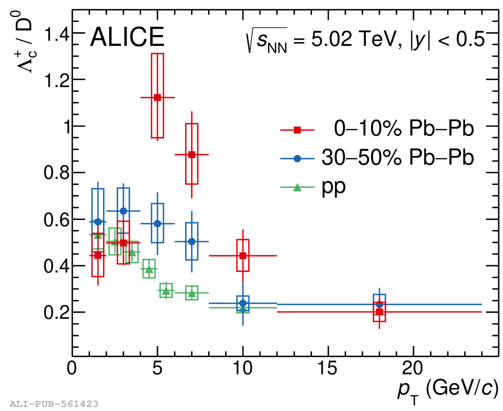

(a)

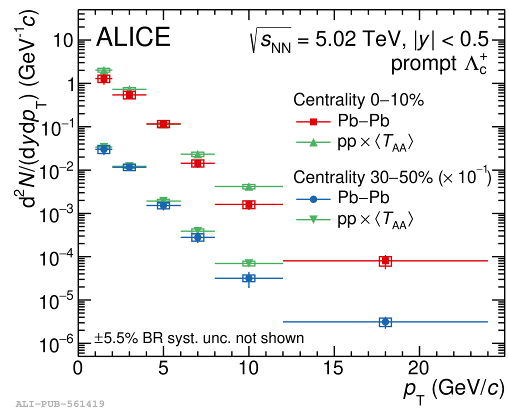

(b)

Figure 10: (a) Λ_c^+/D^0 ratio in central (0-10%) and mid-central (30-50%) Pb–Pb collisions at $\sqrt{s_{NN}} = 5.02$ TeV compared with results in pp collisions.(b) p_T-differential production yields of prompt Λ_c^+ at $\sqrt{s_{NN}} = 5.02$ TeV compared to pp reference. Figures are taken from [44].

3 Monte Carlo Event Generation

Monte Carlo (MC) generators are used to simulate events for different physical processes, providing important comparisons with experimental results. The simulation incorporates the calculation of the cross-section at the parton level at a fixed order in perturbation theory. In MC generators, higher-order corrections are described by parton cascades. Different non-perturbative (soft) effects are described with the help of hadronisation models. Multiple parton interactions (MPIs) are also implemented in some generators. A summary of the complexity of all the processes inside a generated pp collision is illustrated in Fig. 11. In this chapter, various Monte Carlo generators that are used in this thesis are discussed.

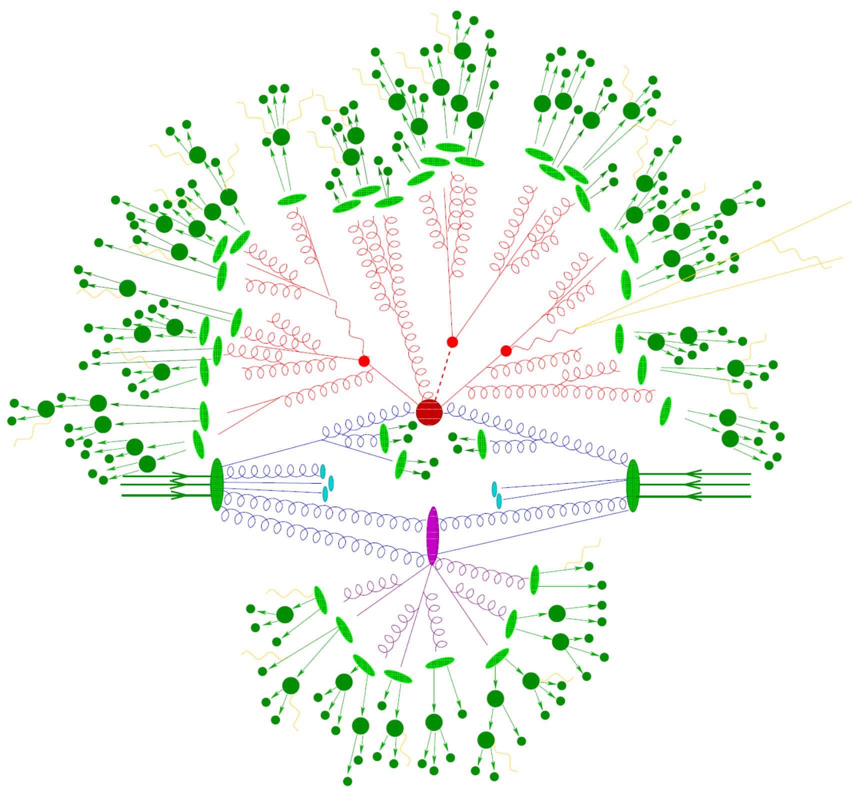

Figure 11: Illustration of a simulated pp collision. The types of processes are: initial state partons (blue), hard scattering processes and their subsequent parton showers (red), the underlying events (violet), and the final state hadrons and their associate decays (dark-green). Figure is taken from [50].

3.1 PYTHIA8

3.1.1 Multiple Parton Interactions

Looking back at Eq. 2.1 it is implicitly assumed that in collisions between two hadrons only two partons, each belonging to one of the hadrons, are taking part in the scattering process, often called SPS: Single Parton Scattering. However, we know that hadrons are composite objects consisting of valence and sea quarks, and gluons. Quantitatively, there is a non-negligible probability that these other partons also participate in the collision. These interactions are called Multiple Parton Interactions and are generally taking place at a lower energy scale than the hard scatterings described by the factorization approach. The MPIs are important and successful in describing the soft underlying events (UE), but it is difficult to describe the produced partons with non-perturbative QCD [24]. UE can be thought of as the result of the interactions between the remnants of the incoming hadrons. UE contribute to the final state by creating new hadrons from hadronisation of outcoming partons, or by interacting with the colour structure of the hard scattering outcoming partons. In Fig. 11 the UE are illustrated in violet.

The invariant masses and the cross sections for the final states of MPI partons increase with increasing collision energies, since partons with lower momentum fraction (Björken-x) are being probed with higher energies, so a large MPI contribution is expected at LHC energies. Here, some of the MPI soft partons can reach an adequate energy scale to produce, through recombination or fragmentation, heavy quarks including charm quarks. It is therefore relevant in heavy-flavour production to include MPI descriptions, which will be discussed for the used generators in the following sections.

3.1.2 Lund String Model

The most commonly used event generators differ in the way that they model hadronisation of partons using non-perturbative calculations. One of the most commonly used hadronisation mechanisms is the Lund phenomenological string model [54], which is the basis of a wide range of Monte Carlo generators. In the Lund model, the interaction between two partons is modeled through colored fields which are represented by strings. The interaction potential of a massless $q\bar{q}$ pair can be described by a Cornell potential

$$V(r) = \kappa r - \alpha r^{-1}, \tag{3.1}$$

which in essence mathematically accounts for quark confinement, containing a Coulomb-like constant α and a string tension term κ. Looking at Eq. 3.1, when the distance r between the quark-antiquark pair increases, the second term becomes negligible and the potential can therefore be approximated as $V(r) \approx \kappa r$, with typically a string tension of 1 GeV/fm. By further increasing the distance between the quark-antiquark pair, the colour string will further stretch due to the linear relation of the stored energy in the strings, and, at a certain point in time, the creation of a new quark-antiquark pair $q_j\bar{q}_j$ becomes energetically more favorable than further extending the string. In Fig. 12a, this string breaking is illustrated.

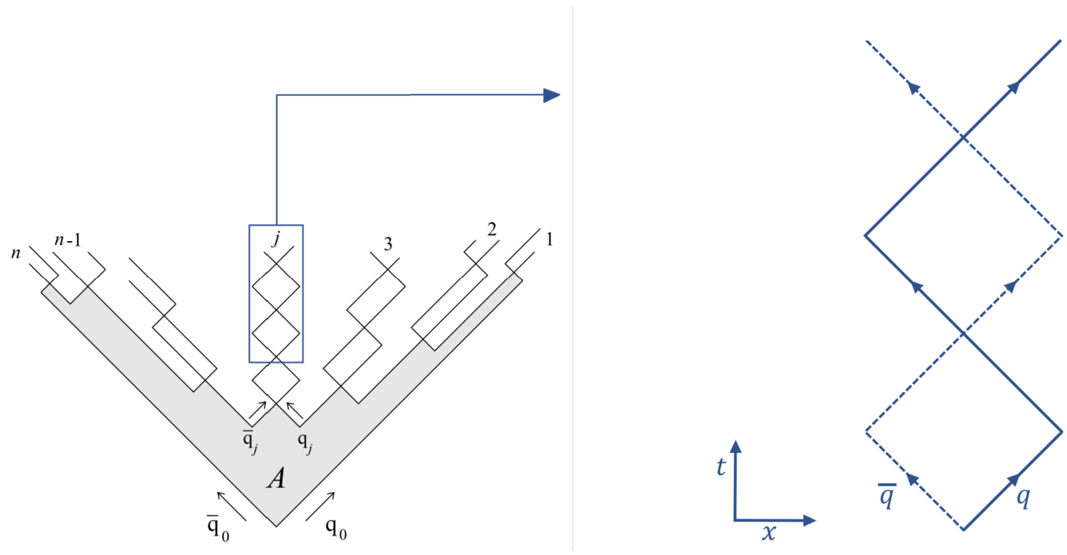

(a) (b)

Figure 12: (a) Illustration of fragmentation of strings in the Lund String Model. Note that massless $q\bar{q}$ pairs without transverse momenta can be produced in a single vertex. (b) Zoomed-in illustration of a single *yo-yo* process in the $x - t$ plane. Figures are taken from [24].

The quark and antiquark with each mass m and transverse momentum $p_\perp$ can not be produced in a single vertex, but the string breaking happens via vacuum tunneling. The probability for the string breaking to happen can be calculated with [53]

$$\mathcal{P}(\text{string breaking}) \propto \exp(-\pi m^2/\kappa)\exp(-\pi p_\perp/\kappa). \tag{3.2}$$

As seen in Eq. 3.2, the production of $q\bar{q}$ pairs strongly scales with the mass of the quarks and antiquarks. The current default suppression of s quark production relative to u and d is 0.217 [53]. The relative charm quark production to the lightest charm flavours is even $1(u) : 1(d) : 1/3(s) : 10^{-14}(c)$, meaning that the production of charm quarks is too heavily suppressed in string breakings. Therefore, heavy flavour $q\bar{q}$ pairs are mainly produced in the hard scattering processes.

Baryons can also be produced in string-breaking processes by the assumption that the string can break by producing a diquark-antidiquark pair in a $\bar{3} - 3$ colour state. The (anti)diquark, with specified spin and flavour, would appear as a new (anti)quark flavour and can combine with a quark or an antiquark to form an (anti)baryon. The different production rates of these baryons would be determined by spin suppression factors and effective diquark masses [55]. Therefore, the creation of pairs of baryons to balance the baryon number gets doubly suppressed. This picture is however modified slightly by considering a step-wise mechanism for baryon production and it is implemented via the *popcorn* model in PYTHIA8 [55].

3.1.3 Colour Reconnection

As discussed, the Lund string model described in the previous section is not able to adequately describe the production rate of baryons. The basic Lund String Model and its fragmentation are implemented completely in the PYTHIA8 Monash 2013 tune which, as seen from Fig. 9b, significantly underestimates the production of Λ_c^+ over D^0. Different theoretical approaches were introduced to describe the enhancement of the baryon-to-meson ratio. In this thesis, enhanced colour reconnection mechanisms will be largely used [57].

The PYTHIA8 Monash tune uses a leading-colour approximation, see Fig. 13a, to trace the colour flow of each event. Each partonic final state contains quarks q_i, with colour index i, that are connected to a single other parton of the event since quarks carry a single (anti-)colour charge. Gluons g_{ij} with colour indices i, j, on the other hand, carry both a colour and an anti-colour charge and hence are connected by colour strings to two partons. The PYTHIA Monash tune was tuned on e^+e^- data. Consequently, this model is effective in describing this collision system, as in non-hadronic collisions, hadronisation primarily occurs through fragmentation. This is due to the lack of slow-moving partons available for recombination. However, this situation can differ significantly in pp collisions where, due to the composite nature of hadrons, we could have MPIs. In the leading-colour approximation, each MPI system will evolve independently and is treated as a separate system. However, all the systems generated are to be considered in the event, and there is a non-negligible possibility of their phase space overlapping. In Fig. 13b, we allow partons from different MPI systems to interact, by merging their colour flow, in order to minimise the total string length, which is also implemented in the PYTHIA8 Monash tune [57].

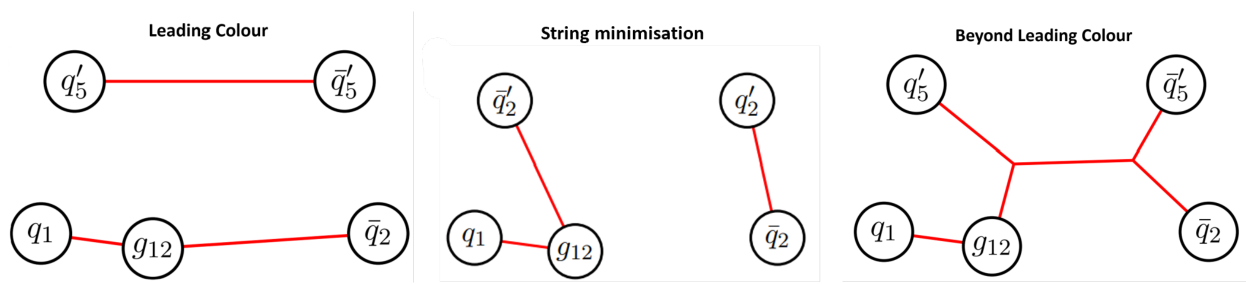

(a) (b) (c)

Figure 13: Parton schemes of (a) leading-colour string topology, (b) MPI-based colour reconnection topology with string minimisation applied, (c) junction beyond-leading-order topologies. Figures are taken from [57].

In the enhanced colour reconnection model in PYTHIA, which is implemented in Colour Reconnection (CR) tunes used in this thesis, the QCD framework is simplified by encoding the parton-parton interaction possibilities in a single colour index from 1 to 9 (and anti-index for anti-colours) [24]. Quarks have a single colour index i, whereas antiquarks have a single anti-colour index. As mentioned, gluons have both a colour index and an anti-colour index, allowing the model to have 9 different quark colour and 72 ($9 \cdot 8$, since the same colour and anti-colour index is not allowed) gluon states. Note that these indices are not the base SU(3) colours of the Standard Model. A colour singlet state is made if the colour index of a quark is equal to the anti-colour index of the antiquark, otherwise, they are in a colour octet state, similar to SU(3) [57].

Specific indices can now combine in pairs to *appear* as new topologies called junctions as the anticolour index which is missing in the triplets [1,4,7], [2,5,8] and [3,6,9]. Walking through the example in Fig 13c: the bottom left quark with colour index 1 can combine with the gluon carrying anti-colour index 1 and colour index 2. The top left quark carries a colour index of 5. Now with this new mechanism, a junction can form between the top left quark and the gluon carrying anti-colour index 8 (since 8 is part of the same triplet). On the right side of the system, the two anti-quarks carrying anti-colour index 2 and 5, can form a junction with colour index 8. Now, since these junctions have opposite colour indices, the junction can combine making the total system again colourless. This mechanism will increase the string topologies that will hadronise since recombinations of quarks are allowed among partons arising from beam remnants and MPIs.

This model predicts the enhancement of charmed baryons, like the Λ_c^+. The achievable topologies in an event are ruled by the minimisation of the string energy, and different modes of the Colour Reconnection (CR) model are possible by tuning various parameters of the model, see Tab. 1. These modes take into account the requirement that, for reconnection to occur between two strings, they must be able to reconnect between their formation and the hadronisation (taking into account time-dilation effects caused by the relative boosts [24]). Looking at Tab. 1, in mode 0 there is no time dilation, and the value of constant m_0 (usually in the order of the Λ_{QCD} scale) controls the amount of colour reconnection. In mode 2, the dipoles involved are all causally connected, and the time dilation is obtained by using a boost factor from the final-state mass of the dipoles [57].

3.1.4 Angantyr

The Angantyr model [59] in PYTHIA8 can be thought of as a generalisation of high energy pp collisions to heavy-ion (HI) collisions, and is used for describing high energy p–A and A–A collisions. To do this, complete exclusive hadronic final states are extrapolated from pp collisions. Similar to PYTHIA8, Angantyr does not include the formation of a thermalised QGP in heavy-ion collisions.
Angantyr is based on the Glauber model [9, 10], where the Good-Walker formalism of diffraction [11] provides a solid description of fluctuations that influence the number of nucleon-nucleon (NN) collisions, and the type of each individual sub-collision in a HI event [14]. The resulting sub-collisions are then simulated with the PYTHIA8 minimum-bias machinery discussed above. From this, elastic, single- and double diffractive, and non-diffractive sub-events are produced. These sub-events are stacked together in the end to form a complete HI event. In this thesis, we will study different hadronisation models implemented in Angantyr. Firstly we study the effects of CR in heavy-ion collisions, where all sub-collisions hadronise (via string fragmentation) individually [14], assuming that the colour dipoles that build up the string in different sub-collisions do not interact with each other [15].

Parameter	Monash	Mode 0	Mode 2
StringPT:sigma	0.335	0.335	0.335
StringZ:aLund	0.68	0.36	0.36
StringZ:bLund	0.98	0.56	0.56
StringFlav:probQQtoQ	0.081	0.078	0.078
StringFlav:probStoUD	0.217	0.2	0.2
StringFlav:mesonCvector	0.88	0.88	0.88
	0.5	0.0275	0.0275
StringFlav:probQQ1toQQ0join	0.7	0.0275	0.0275
	0.9	0.0275	0.0275
	1.0	0.0275	0.0275
MultiPartonInteractions:pT0Ref	2.28	2.12	2.15
BeamRemnants:remnantMode	0	1	1
BeamRemnants:saturation	–	5	5
ColourReconnection:mode	0	1	1
ColourReconnection:allowDoubleJunRem	on	off	off
ColourReconnection:m0	–	2.9	0.3
ColourReconnection:allowJunctions	–	on	on
ColourReconnection:junctionCorrection	–	1.43	1.20
ColourReconnection:timeDilationMode	–	0	2
ColourReconnection:timeDilationPar	–	–	0.18

Table 1: List of all the parameters among the PYTHIA8 tunes considered in this thesis, taken from [57].

3.2 HERWIG7

The Hadron Emission Reactions with Interfering Gluons (HERWIG) generator [98] is a general-purpose generator that can perfom matrix-element calculations beyond leading order in QCD, while it keeps its ability to describe Beyond Standard Model (BSM) events, cluster hadronisation models and parton showers [24, 60]. HERWIG works for all standard model processes and uses the coherent branching algorithm to develop its parton showering [61] and, in the latest version, the generator introduced heavy-quark fragmentation via mass-dependent splitting functions and a covariant formulation of the shower algorithm [62]. In HERWIG7, the hadronisation of quarks and gluons happens via a cluster model called after the parton showering. After the parton shower, the remaining gluons are split non-perturbatively into quark-antiquark pairs, with any flavour. Due to the isotropic decays during the event, only partons that are in colour singlet states, defined with the cluster algorithm, are created with the momentum given by the sum of the momenta of the constituent [24]. Due to the colour-preconfinement property, these clusters have a mass distribution that is independent of the centre of mass energy and the initial hard scattering process [24]. The mass spectra are peaked at low masses and are universal, meaning that the clusters can be seen as excited hadron resonances, and can decay to the observed hadrons according to the phase space. There is however a small fraction of clusters that are too heavy for this, so they are split into lighter clusters before the decay. These heavy clusters split (cluster fission) into two clusters if the cluster mass M is such as [62]

$$M^{\mathrm{Cl_{pow}}} \geq \mathrm{Cl}_{\max}^{\mathrm{Cl_{pow}}} + (m_1 + m_2)^{\mathrm{Cl_{pow}}}, \tag{3.3}$$

where $\mathrm{Cl_{max}}$ and $\mathrm{Cl_{pow}}$ are parameters of the model (flavour dependent values), and $m_{1,2}$ are the masses of the partons in the cluster. For heavy clusters that need to be split, a quark-antiquark pair is selected from the vacuum and popped. Once the pair is selected, the cluster can decay into two lighter clusters with one of the initial partons in each cluster, with mass distributions $M_{1,2}$

$$M_{1,2} = m_{1,2} + (M - m_{1,2} - m_q)\mathcal{R}_{1,2}^{1/P}, \tag{3.4}$$

with again $m_{1,2}$ the masses of the initial partons, m_q the mass of the parton taken from the vacuum and M the mass of the original cluster. The distribution of the cluster masses is controlled by the parameter P, which is `PSplitCharm` for clusters containing a charm quark. Furthermore, a soft distribution is used for the masses of clusters resulting from splitting if the heavy clusters contain a particle from the beam remnant. The last step of the cluster hadronisation is the decay of a cluster into a pair of hadrons. For a given cluster with flavour $(q_1, \bar{q_2})$ a quark-antiquark $(q, \bar{q})$ or diquark-antidiquark pair $(qq, \bar{q}\bar{q})$ is extracted from the vacuum and is combined, such that a pair of hadrons is formed with flavours $(q_1, \bar{q})$ and $(q, \bar{q_2})$. It is also possible to form baryons. The final hadrons are then selected from all possible hadrons with the appropriate flavours based on the phase space, flavour of the constituents and the spin.
Similar to other Monte Carlo models, HERWIG uses weights for the production of hadrons $a_{(q_1,\bar{q})}$ and $b_{(q,\bar{q_2})}$ through cluster decays, which are calculated as

$$W(a_{(q_1,\bar{q})}, b_{(q,\bar{q}_2)}) = P_q w_a s_a w_b s_b p^*_{a,b}, \tag{3.5}$$

where P_q is the weight for the production of the selected quark-antiquark or diquark-antidiquark pair, $w_{a.b}$ the weights for the production of the individual hadrons and $s_{a,b}$ are the suppression factors for the hadrons. A lot more mesons are produced in the model than baryons, so to increase the baryon production, $s_{a,b}$ will select whether the cluster will perform a mesonic or baryonic decay, depending on if the cluster is heavy enough to form the lightest baryon-antibaryon pair. The last factor $p^*_{a,b}$ measures the phase space available for the two-body decay through the momentum of the formed hadrons.

There are in total three colour reconnection models implemented in HERWIG: the default plain reconnection model (PR) [62, 64], the baryonic reconnection model (BR) [66] which allows the formation of baryonic clusters and a more complicated statistical model [65]. Both the PCR and the statistical model in HERWIG only deal with mesonic clusters, so an extension was needed to the reconnection algorithm to produce baryonic clusters via reconnection. Since the baryonic clusters will have a large invariant mass, the BR model will not use a similar reduction of the cluster masses, but it will use a geometric approach of the nearest neighbors in which the reconnection is performed in the same phase space region based on the rapidity y[2]. In Fig. 14a the formation of two baryonic clusters out of three mesonic clusters close in phase space is illustrated.

[2]Rapidity is a kinematic variable, which can be defined as $y = \frac{1}{2}\ln\left(\frac{E+p_z}{E-p_z}\right)$, where p_z is the longitudinal momentum and E is the energy.

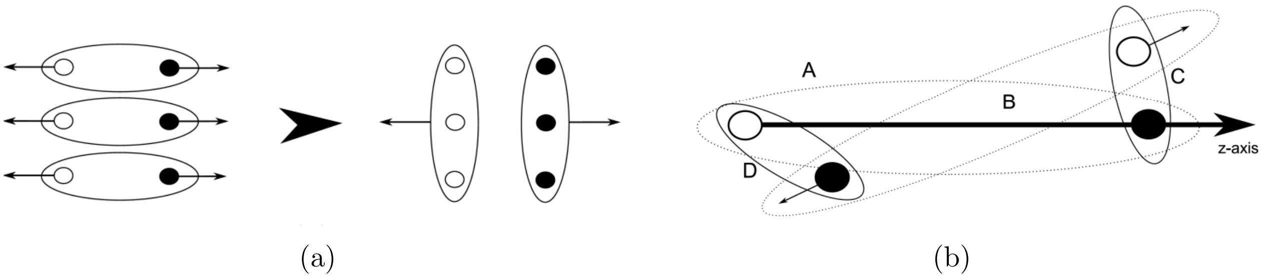

Figure 14: (a) Configuration of clusters that might lead to baryonic reconnection. (b) Illustration of rapidity-based colour reconnection, where the quark axis of one cluster is defined as the z-axis. Clusters A and B are the original clusters and C and D are the new ones after reconnection. Figures are taken from [66].

Fig. 14b shows the rapidity-based reconnection for both mesonic and baryonic clusters. Note that Fig. 14a shows how reconnection can only happen if all the quarks (and anti-quarks) move in the same direction.

In HERWIG7 the description of the MPIs is based on the eikonal multiple parton-parton scattering model [67], which describes the MPIs as additional soft partonic and semi-hard interactions. In HERWIG, a generic high-momentum transfer process generating coloured particles follows a perturbative evolution from the hard scale of the collisions to an infrared cutoff region [24]. At LHC energies, the MPIs are dominant in the perturbative regime above this cutoff scale, and create additional parton showers. Furthermore, non-perturbative partonic scatters are included below this scale, which makes it possible to simulate underlying events (UE) and minimum bias (MB) events in hard scattering events. By adding MPI based CR to the BR model, a significant improvement in the production of charmed baryons is observed [66]. For this reason, MPI based CR is included in the BR and PR model in this thesis.

3.3 EPOS4

3.3.1 Parton Based Gribov Regge Theory

The Parton Based Gribov Regge Theory (PBGRT) [68] merges two separate theoretical frameworks, the Parton Model (PM) and Gribov-Regge Theory (GRT), and is the theoretical basis of EPOS. The model aims to describe both hard and soft processes properly. The central concept of this theory is to have a realistic description of all processes during a collision using multiple scatterings, where we care explicitly about the fact that the total energy should be distributed among all the separate individual interactions. In EPOS, all types of interactions are allowed, such as pp, p–A, and Pb–Pb. With this approach, cross-sections and particle productions can be determined, while accurately taking energy conservation into account. In essence, the EPOS4 generation is based on connecting four fundamental concepts: energy- and momentum conservation (via energy sharing), parallel scattering, factorisation and saturation. EPOS4 uses an S-matrix approach to accumulate all four concepts. For further reading, see [72, 73, 78].

3.3.2 Core, Corona and Strings

In EPOS, the pomeron or parton ladder represents the elementary interaction between partons. The cut pomerons that are produced in the parton interactions are mapped to relativistic strings [72]. The string is identified as a quark-antiquark pair with the same flavour linked by a chain of gluons, thus forming a chain of the form $q-g-\cdots-g-\bar{q}$. When a string is formed of a $q-\bar{q}$ pair, the string is a longitudinal object, but adding (emitted) gluons can add a transverse dimension to it via so-called transverse kinks. These types of strings are known as kinky strings, as illustrated in Fig. 15, where we suppose e^+e^- annihilation.

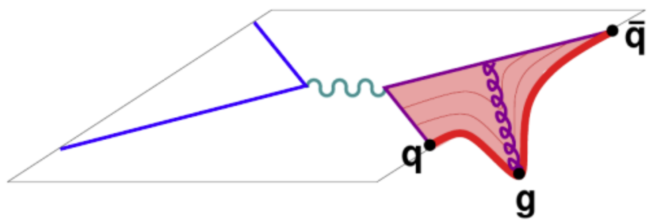

Figure 15: An illustration of a kinky string formed by a final state $q-\bar{q}$ pair created in e^+e^- annihilation where a transverse gluon is emitted. Figure is taken from [70].

Similar to PYTHIA, the initial partons have some momenta and the string will be stretched as they expand, which will lead to an increase in its potential energy due to its tension. As the string stretches, it is at some point more favorable to use the energy to produce a new $q\bar{q}$ pair, of the same flavour, rather than stretching the string even further. The string will split into two segments, which will in turn evolve and fragment, thus reducing their tension after each breaking. It is also possible to create diquark-diantiquark pairs at a breaking point. We note here that it is possible to have any quark flavour on the end of the parton chain, but only the light quark flavours (u, d and s) can be produced at the breaking points, because of kinematic reasons. The breaking points on a string are calculated following the so-called Area Law [71]. Note here that a high-transverse momentum pQCD process in EPOS4 also contributes to particle production with low p_{T}, since only kinky strings that break close to the high-p_{T} kink will produce high-p_{T} particles.

It is also possible to have a certain dense environment where the string segments can not evolve into hadrons. We will denote these segments as prehadrons, and the segments can *fuse* to produce the *core*, or they can form hadrons when they escape from it. This is also true for excited remnants. These prehadrons will undergo a *core-corona* procedure, allowing us to identify the core that can be treated as a fluid early in the evolution at time τ_0, which is a parameter in the model [75]. The procedure consists of checking, where the local string density ρ is larger than a critical density value ρ_0, if the prehadron has a minimal transverse momentum $p_{\mathrm{T}}^{\mathrm{new}}$ to escape:

$$p_{\mathrm{T}}^{\mathrm{new}} = p_{\mathrm{T}} - f_{E_{\mathrm{loss}}} \int_{\gamma} \rho \, \mathrm{d}L, \tag{3.6}$$

where p_{T} is the initial transverse momentum of the prehadron, $f_{E_{\mathrm{loss}}}$ is a constant (more details in [74]) and γ is the hypothetical trajectory of the string segment [76]. If the computed value for $p_{\mathrm{T}}^{\mathrm{new}}$ is positive, the string segment will escape the core and be part of the *corona*, where it will evolve and fragment as described above. Corona particles are either close to the surface or highly energetic (these move out from the center) particles, or a combination of both, and can be treated with microcanonical hadronisation [74]. An important feature in EPOS is that the target and projectile remnants are left off-shell, and eventually will contribute to the particle production at large rapidity as part of the corona [77]. For $p_{\mathrm{T}}^{\mathrm{new}} \leq 0$, the prehadron is considered to be a core *prehadron*.

To reproduce the fluid-like behaviour of the QGP, the core will evolve using viscous relativistic hydrodynamics. In EPOS, there are two choices for the equation of state (EoS) for the hydrodynamic treatment of the core. The one used in this thesis is called *cross-over, 3 flavour conservation* (x3ff), which includes a cross-over transition between an ideal QGP and a hadron resonance gas [79]. This mode is parameterized to match lattice QCD calculations at vanishing chemical potentials [69, 76].

At this stage, the hadrons formed from both the corona and the core are in a dense gaseous environment, in which they can interact. The hadronic cascades, or the so-called hadronic rescattering (Hacas), are simulated with the Ultra-relativistic Quantum Molecular Dynamics (UrQMD) transport model [82, 83], where the hadrons scatter elastic- and inelastically. For each scattering simulated with UrQMD, the cross-sections either come from experimental measurements or are calculated with the Additive Quark Model (AQM) [84]. The rescattering involves particles from fluid hadronisation, but also corona particles from hard processes. Rescattering reduces significantly low p_{T} yields for baryons, due to baryon-antibaryon annihilation [74]. These scatterings will last until the system undergoes a complete freeze-out, and the final-state hadrons will continue their free streaming, where they will undergo some late weak decays eventually.
In EPOS4 heavy quarks do not interact with the medium, and heavy hadrons are mainly produced by fragmentation functions, described by $\mathrm{e^+e^-}$ collisions [81]. In the newer EPOS4HQ version [80], the heavy quarks can interact with partons of the QGP, which are gluons and lighter quarks from the core to form heavy mesons and baryons. In this model, the creation of a QGP in high energy density regions is allowed in some spatial regions where the energy density of the fluid is above a critical density, even in smaller-size systems. This means that the heavy quarks can hadronise via fragmentation and coalescence. The coalescence contribution changes the observables in medium and high multiplicity pp collisions as compared to low multiplicity and observed in $\mathrm{e^+e^-}$ collisions. For example, EPOS4HQ shows a strong enhancement of the $\Lambda_{\mathrm{c}}^{+}/\mathrm{D}^{0}$ ratio at low p_{T} for higher multiplicity pp collisions and describes the experimental data adequately [81]. While writing this thesis only the default EPOS4 version is available.

4 Charmed hadron production studies

4.1 RIVET analyses

The first aim of this thesis is to compare the measurements from recent ALICE results on prompt charmed baryon and meson production in pp at $\sqrt{s} = 5.02$ TeV and $\sqrt{s} = 13$ TeV, and in p–Pb and Pb–Pb at $\sqrt{s_{\mathrm{NN}}} = 5.02$ TeV. As part of this thesis, I led and contributed to the development of several RIVET analyses needed for published ALICE results. These analyses were validated by the ALICE collaboration MC analysis group. Since RIVET is a vital part of the analysis, I will briefly introduce the fundamentals behind the framework in the following section. The analysis will include the rivetisations of the following recent papers by ALICE, with their respective RIVET identifiers:

- `ALICE_2023_I1990765`: Constraining hadronization mechanisms with Λ_c^+/D^0 production ratios in Pb–Pb collisions at $\sqrt{s_{\mathrm{NN}}} = 5.02$ TeV [44].
- `ALICE_2022_I2593302`: First measurement of Λ_c^+ down to $p_{\mathrm{T}} = 0$ in pp and p–Pb collisions at $\sqrt{s_{\mathrm{NN}}} = 5.02$ [39].
- `ALICE_2022_I2025044`: Measurement of beauty production via non-prompt D^0 mesons in Pb–Pb at $\sqrt{s_{\mathrm{NN}}} = 5.02$ TeV [36].
- `ALICE_2021_I1946131`: Prompt D^0, D^+ and D^{*+} in Pb–Pb collisions at $\sqrt{s_{\mathrm{NN}}} = 5.02$ TeV [35].
- `ALICE_2021_I1848990` (contributed): Measurement of beauty and charm production in pp collisions at $\sqrt{s} = 5.02$ TeV via non-prompt and prompt D mesons [33].
- `ALICE_2021_I1862793`: Measurement of the cross sections of Ξ_c^0 and Ξ_c^+ baryons and branching-fraction ratio $\mathrm{BR}(\Xi_c^0 \to \Xi^- e^+ \nu_e)/\ \mathrm{BR}(\Xi_c^0 \to \Xi^- \pi^+)$ in pp collisions at 13 TeV [41].
- `ALICE_2021_I1868463` (not contributed): Measurement of prompt D^0, Λ_c^+, and $\Sigma_c^{0,+,++}(2455)$ production in pp collisions at $\sqrt{s} = 13$ TeV [40].
- `ALICE_2023_I2697877`: Charm production and fragmentation fractions at midrapidity in pp collisions at $\sqrt{s} = 13$ TeV [37].

4.1.1 Introduction to RIVET

With the fast development of Monte Carlo generators, more mechanisms in these models are added to improve the agreement with the experimental results. However, some of these might harm previously achieved compatibilities. We can overcome this challenge by comparing many published results with experimental data [86]. The Robust Independent Validation of Experiment and Theory (RIVET) framework provides a (universal) way to reproduce the experimental results with the output of Monte Carlo generators [85]. Fig. 16 shows how the RIVET framework connects the theory underlying a model with experimental results. One can see that the comparisons with RIVET are a back loop to phenomenological models making them a perfect tool for the development, validation and tuning of Monte-Carlo generators [87]. Furthermore, RIVET is used by different LHC experiments as a part of their analysis and experimental interpretation [88], and it can also be used in studies of future experiments [89].

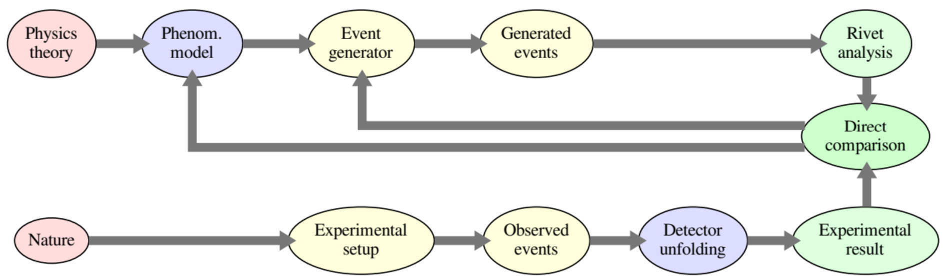

Figure 16: Block diagram of the way RIVET connects theory and validation with experimental results. Figure taken from [86].

The RIVET framework is based on a C++ and Python shared library [90]. It is able to read events stored in HepMC format (available by default for PYTHIA8, HERWIG7 and EPOS4) [94] which is used as the input of a RIVET analysis, as seen in Fig. 16. The user thereafter creates a single C++ macro, independently of the generator that is used. One of the key ingredients in building a RIVET plugin is the projection. A projection is a stateful object that is inherited from the `RIVET::Projection` class [25]. It is used to extract physical observables from generated events, for example: final-state or unstable particles meeting specific particle identification or kinematic requirements, event centralities, event multiplicities, etc. Normally, these selections need to be repeated for each particle separately in the analysis, while in RIVET this is done by pre-calling the projections. It is therefore also the responsibility of the user to use the same kinematical and identification cuts applied in the published analysis, to ensure a proper comparison. The RIVET macro can be split into three main parts, which are implemented by the user as separate member functions in the analysis class. An illustration of the analysis class in RIVET is shown in Fig. 17. The three functions are consecutively:

- **Initialization**: The first method `init()` is used to set up the analysis, and is called once at the beginning of the analysis. This method is used to initialize the histograms with the correct types and binnings via the `RIVET::book()` function. To compare Monte Carlo-generated events with published data, one can also use RIVET to book histograms with corresponding reference data. Furthermore, all the aforementioned projections can be defined in this method.

- **Analysis**: The method `void analyze(const RIVET::EVENT& event)` is used for filling histograms and calculations of variables at each event with the applications of the projections. This method is therefore called for each event.

- **Finalization**: The method `finalize()` is only called at the end of the analysis. The user can implement normalization and scaling of the filled histograms in this part. Some observables may be averaged in this part which can be used, for example, for scaling the production cross section and calculating the R_{AA}. To calculate the latter, one needs to merge runs from different collision systems. One can do this by setting `Reentrant:True` in the .info file of the RIVET analysis.

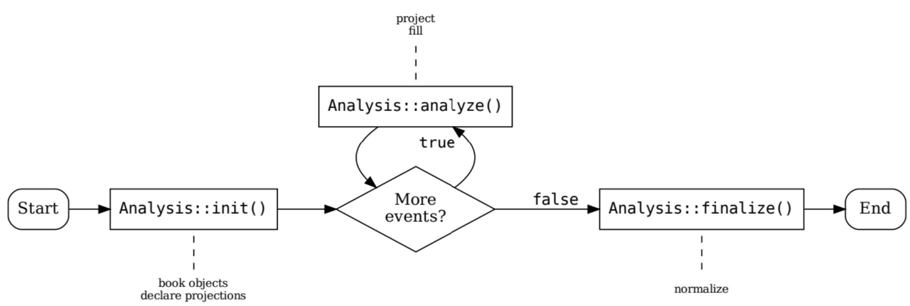

Figure 17: The execution flow of the `Analysis` class in a RIVET analysis. Figure taken from [86].

4.2 Observables

In this part of the thesis, several experimental observables are inspected which are commonly used as probes to study charmed hadron production. The observables of interest in pp collisions at mid-rapidity are the p_{T}-differential production cross section, ratios between prompt/non-prompt charmed mesons, the baryon-to-meson ratio and the baryon-to-baryon ratio between different prompt charmed hadron species. The baryon-to-meson ratios of interest are prompt Λ_c^+/D^0, Ξ_c^+/D^0, Ξ_c^0/D^0, and $\Sigma_c^{0,+,++}/\mathrm{D}^0$. These ratios measured at mid-rapidity show significant deviations from the values reported in e^+e^- collisions, and the Monash Tune of PYTHIA8 generally underpredicts the production rates of the charmed baryons. It is therefore interesting to study these ratios with different Monte Carlo generators since we need further hadronisation effects, apart from pure in-vacuum fragmentation, to describe the measurements of charmed baryon production. The prompt baryon-to-baryon ratios of interest are Ξ_c^0/Λ_c^+, $\Xi_c^{0,+}/\Sigma_c^{0,+,++}$ and $\Lambda_c^+(\leftarrow \Sigma_c^{0,+,++})/\Lambda_c^+$, since we want to study the suppression of spin-1 diquarks to spin-0 diquarks inside string hadronisation frameworks [40] and cluster models. Also, the non-prompt to prompt ratio of D^0, D^+, D^{*+} and D_s^+ are looked at. These observables are studied at either $\sqrt{s} = 5.02$ or 13 TeV, depending on the RIVET analysis done of the respective paper. Most of the D-meson and Σ_c primary particle spectra are used to tune parameters related to charmed meson production in PYTHIA8 CR Mode 2, see Sec. 6.

In p–Pb at $\sqrt{s_{\mathrm{NN}}} = 5.02$ TeV, we study the nuclear modification factor R_{pPb} of Λ_c^+ to examine possible modifications of their production due to the potential presence of cold nuclear effects with respect to pp collisions. Also, we inspect the p_T-differential cross section of Λ_c^+ and D^0, and subsequently the p_T-dependent Λ_c^+/D^0 ratio. We compare the p_T-integrated Λ_c^+/D^0 ratios between p–Pb and pp collisions. We extend this study to central (0-10%) and mid-central (30-50%) Pb–Pb collisions at $\sqrt{s_{NN}} = 5.02$ TeV, where we include the p_T-differential yields for D-mesons. Furthermore, we calculate the p_T-dependent average nuclear modification factor R_{AA} of D-mesons.

4.3 Methods

4.3.1 RIVET analysis

For this thesis, the Rivet versions 3.1.8 and 3.1.9 were used. For the analyses in pp events at mid-rapidity ($|y| < 0.5$), particles with a low transverse momentum $p_T > 0$ GeV/c are considered. However, for some rivetisations, the range of the transverse momentum was set to $p_T > 2$ GeV/c. In the `init()` method, these selections are implemented via the `UnstableParticles` projection, since we want to project out all physical (but decayed) particles in an event. In this thesis, mainly prompt particles are considered, thus the particles that are produced directly in the hadronisation of a charm quark (in the hard scattering) or the strong decay of a directly produced excited charm-hadron state. For the analysis of non-prompt D-mesons, we only include particles that are produced in the decay of particles containing a beauty quark. The histograms are normalized to obtain the p_T-differential production cross sections per unit rapidity. By integrating over the respective p_T-range, we calculate the p_T-integrated production cross section. Furthermore, we use the cross sections to calculate the aforementioned meson-to-meson, baryon-to-meson and baryon-to-baryon ratios.

Fig. 18 shows, as an example, a comparison between measurements by the ALICE experiment of the p_T-differential cross section prompt D^0 and Λ_c^+ at mid-rapidity in pp collisions at $\sqrt{s} = 5.02$ TeV with data from the Monte Carlo generators discussed in the previous section. In Fig. 18a, the data generated by models is smoothed with a parameterized Bezier curve [92].

In p–Pb, only events with unstable particles in the rapidity range $-0.96 < y_{cms} < 0.04$ are considered. This rapidity range is shifted due to the asymmetry of the colliding beams. Again, in the `init()` method, these cuts will be implemented via the `UnstableParticles` projection. To calculate the R_{pPb} we can divide the obtained yields from p–Pb and pp (and scale this with the atomic number of lead, $A = 208$) respectively, as in Eq. 1.8. We can only do this by merging event generations with both pp and p–Pb collisions. By setting `Reentrant:True` in the .info file of the RIVET analysis, RIVET will then re-run the `finalize()` method, and the R_{pPb} will be calculated accordingly.

The RIVET analysis in Pb–Pb collisions is very similar to that of the p–Pb system. However, instead of studying the production of unstable particles for mid-rapidity events, we want to inspect two centrality classes 0-10% (central) and 30-50%. The centrality is an experimental quantity to characterize heavy-ion collisions. It quantifies the overlap between the two colliding nuclei during a collision using a percentage scale (with 0% head-on, and 100% means

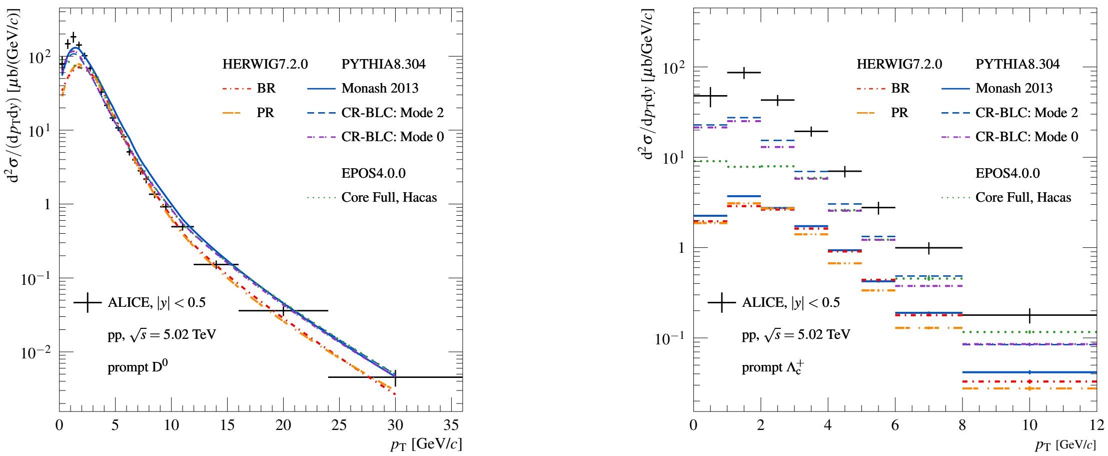

(a) (b)

Figure 18: Measurements of the p_T-differential production cross sections of (a) prompt D^0 [33] and (b) prompt Λ_c^+ [39] by the ALICE experiment, compared with data from PYTHIA8, HERWIG7 and EPOS4.

no overlap). The centrality can therefore relate to the impact parameter b. In ALICE, the centrality determination is provided by the total signal measured in the V0 detector [93], consisting of two arrays, V0-A and V0-C, which cover respectively the pseudorapidity ranges $2.8 < \eta < 5.1$ and $-3.7 < \eta < -1.7$. In Fig. 19a, the distribution of the sum of the amplitudes in the V0 scintillation detectors for Pb–Pb is shown. The most central collisions, associated with 0-1%, correspond to the events with the highest V0 amplitude. See for more details on centrality determination in ALICE [8]. In RIVET, the centrality determination uses the multiplicity of charged particles in the acceptance of the V0 detector. Since different models result in different multiplicity distributions, it is necessary to create calibration files for different energies and event generators. Fig. 19b shows the V0 amplitude distribution measured by ALICE in black and the multiplicity distribution of charged particles in Pb–Pb collisions at $\sqrt{s_{NN}} = 2.76$ TeV generated with PYTHIA8 Angantyr (red), which is calculated with RIVET. To build centrality classes, RIVET divides the charged particle multiplicity distribution into centrality percentiles. The most central events (0-1%) correspond to the highest multiplicity events.

Before we run a Pb–Pb analysis in RIVET, we preload a calibration file (in YODA format). This calibration can be implemented with a centrality projection. A similar process is currently under development in RIVET for multiplicity determination in pp and p–Pb collisions [91]. We use this projection to filter out the events with incorrect centrality values. To calculate the R_{AA} we can divide the obtained yields from Pb–Pb and pp (and scale this with the number of binary nucleon-nucleon collisions, $\langle N_{coll} \rangle$) respectively, as in Eq. 1.6. The correct value of $\langle N_{coll} \rangle$ can be taken from [8] for each centrality class.

The calculation and propagation of statistical errors in the event generator modeling is done by assigning a set of different weights for each generated event corresponding to, for example,

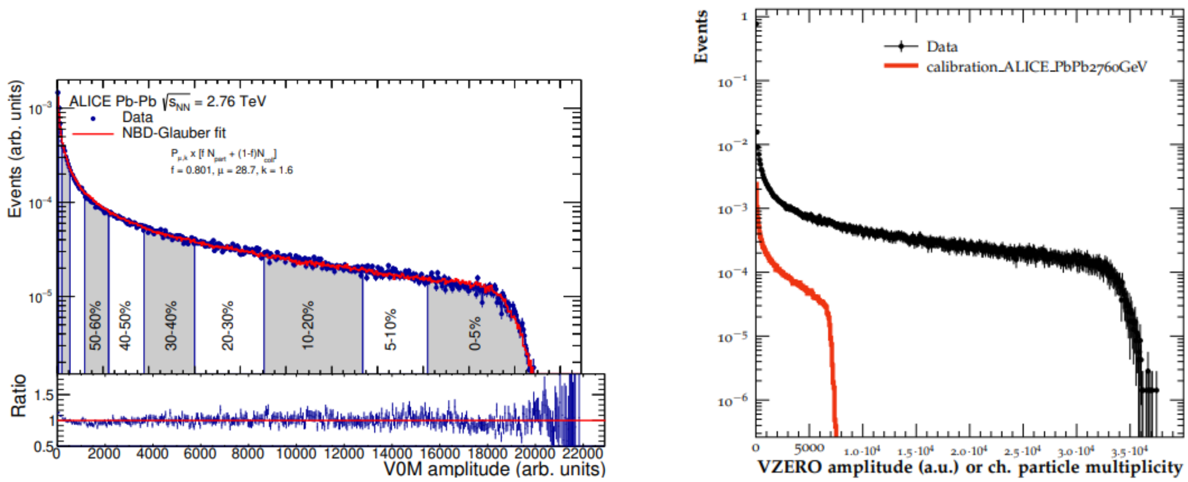

(a) (b)

Figure 19: (a) Distribution of the sum of amplitudes in V0 scintillators in Pb–Pb collisions at $\sqrt{s_{\mathrm{NN}}} = 2.76$ TeV (blue), with the NBD-Glauber fit (red line). (b) Charged particle multiplicity calculated with RIVET from Pb–Pb collisions at $\sqrt{s_{\mathrm{NN}}} = 2.76$ TeV generated with PYTHIA8 Angantyr (red line), V0 amplitude distribution in arbitrary units measured by ALICE (black markers). Figures are taken from [8] and [91] respectively.

different scale choices. There is a system of combining events in an event group. Each bin in a histogram of a soft/or collinear safe observable will be filled once by each such event group, with a weight given by the sum of the weights of the counter-events and real events [85]. These fills have the correct error propagation encoded in the sum of squared weights and the sum of weights. In the used RIVET versions, the weight handling is implemented behind the scenes and handled automatically. In RIVET, the estimation of errors is correctly extended to correlated observables, see [85].

4.3.2 Simulation setup

In this thesis PYTHIA8.304 is mainly used to simulate minimum bias (MB) pp collisions at $\sqrt{s} = 5.02$ TeV and $\sqrt{s} = 13$ TeV. For the generation of p–Pb and Pb–Pb events, we will use Angantyr. To simulate minimum bias events in PYTHIA8 with the default Monash 2013 Tune, we set `SoftQCD:all = on` to enable different Soft QCD processes in PYTHIA8, like non-diffractive (inelastic), single diffractive, elastic and double diffractive processes [96]. We will not consider hard QCD processes and disable Initial- and Final State Radiation. On the other hand, Multi-Parton Interactions are enabled. This PYTHIA8 setup was also (mainly) used in the rivetised ALICE papers. Besides the default Monash 2013 tune, Colour Reconnection (CR) Mode 0 and Mode 2 (based on [57]) were also used to generate pp collisions. The additional parameters are found in Sec. 3.1.3, and we will set `SoftQCD:all = on` to also allow for all Soft QCD processes. For all PYTHIA8 tunes, 100 million pp collisions are generated.

In Angantyr, one needs to add the `HeavyIon:mode 1` parameter to the PYTHIA8 macro to run minimum bias p–Pb events, and set the correct beam PID. To run Pb–Pb events, we need to preload a calibration file corresponding to the right event generator and energy. We will use the GLISSANDO Woods-Saxon model to describe the distribution in the radial density of nucleons in a nucleus [97]. This is the default nucleus model in Angantyr and it works well for large nuclei. Besides this, QCD CR Mode 0 and 2 parameters (see Tab. 1) were also added to study additional colour reconnection mechanisms in heavy-ion collisions, which is applied on every sub-collision individually, see Sec. 3.1.4. The latter is simulated with PYTHIA8.304/Angantyr. For heavy-ion collisions, around 10 million events are generated with p–Pb collisions and 1 million with Pb–Pb collisions.

One can take the parameters for the correct PR (default)- and BR configurations from [99] to run minimum bias pp collisions with HERWIG7 using both the Plain Reconnection (PR) and Baryonic Reconnection (BR) tune (as described in Sec. 3.2). Besides this, MPI based CR is included, and the Soft Tune model [99]. Lastly, we set the strange quark mass to 0.45 * GeV to allow for alternative gluon splitting to $s\bar{s}$ pairs. Hence, the PR and BR use similar parameters, except for the (Baryonic) Reconnection Probability parameters, to enhance baryon production. For both HERWIG7 tunes, 100 million pp collisions are generated.

To run minimum bias events in EPOS4, one needs to set up the *option* file. In all the studied collision systems, we set the parameter *application* to hadron, which includes the hadron-hadron, nucleus-nucleus, and hadron-nucleus scatterings. One could also choose to set *application* to ee, for e^+e^- collisions, or with a decay of kinky strings by setting *kinky*. We can *tune* EPOS4 in different ways, by enabling and disabling different components. Those are: core/corona (*core*), the hydrodynamical evolution of the core (*hydro*), the equation of state (*eos*), and the hadronic cascade (*hacas*). In this thesis, different combinations of components are tested. The most promising results for the study of charmed hadrons in pp collisions are only reported. Lastly, to simulate minimum bias events, we set the *centrality* value to 0. Comparisons with EPOS4 are not available for observables involving Σ_c baryons and D^{*+} mesosns because their lifetimes are shorter than 10^{-19} seconds. As a result, these events are not recorded by default. Due to time contraints of the project, no EPOS4 comparisons in heavy-ion collisions are present in the thesis.

5 Results and discussion on charm production studies

In this section, we present an important review of the latest Monte Carlo models available applied to recent ALICE results. The p_T-differential production cross sections of individual particles are presented in Appendix A. Generally, measurements by the ALICE collaboration are compared with string models implemented in PYTHIA8 with the Monash Tune, QCD-CR Mode 0 and QCD-CR Mode 2 tunes. Also, we show comparisons with cluster models implemented in HERWIG7, with the Plain Reconnection tune (PR) and Baryonic Reconnection model (BR). At last, EPOS4 enabled with hadronic rescattering and the full core/corona mechanism are compared with the data. No other EPOS4 mechanisms (or combinations thereof) are shown, due to the larger disagreement with the experimental measurements. Simulation results will be commented on for each generator for all measurements.

5.1 Charmed hadron production study in pp collisions

5.1.1 Meson-to-meson ratios

A subset of the p_T-differential production cross sections of prompt and non-prompt D-mesons measured at midrapidity ($|y| < 0.5$) in pp collisions at $\sqrt{s} = 5.02$ TeV by the ALICE experiment [33] is presented in Fig. 33. The meson-to-meson ratios of both non-prompt and prompt $D_s^+/(D^0 + D^+)$ measured at $|y| < 0.5$ in pp collisions at $\sqrt{s} = 5.02$ TeV is presented in this section in Fig. 20. These are compared with MC generators mentioned in Sec. 4.3.2.

All the PYTHIA8 tested tunes describe well the measurements of both non-prompt and prompt $D_s^+/(D^0 + D^+)$ meson-to-meson ratios within uncertainties and follow the general trend. For $p_T > 10$ GeV/c, the predictions generally underestimate data for prompt D-mesons. A relatively higher production rate for D-mesons is observed in PYTHIA8 Monash relative to QCD-CR Mode 0 and Mode 2 for low-p_T. The majority of the production of baryonic junction reconnections comes from color dipoles along the beam axis, resulting in a higher overall baryon production at lower p_T, potentially suppressing the available phase space for D-meson production. The effects on the p_T of the partons produced by MPI are smaller for higher p_T, hence the differences between Monash and the QCD-CR tunes are smaller in this region. In both ratios, a relatively flat trend is observed for all three PYTHIA8 tunes, implying that strangeness is not enhanced in the formation of mesonic junction topologies, but strange quarks are similarly suppressed across the different tunes for pseudoscalar D-mesons.

In Fig. 21, the prompt D^+/D^0 and D^{*+}/D^0 meson-to-meson ratios are presented. For all PYTHIA8 tunes, the relative production for D^+/D^0 is approximately 0.5, slightly overestimating the experimental measurements. One can observe that in general all PYTHIA8 tunes underestimate the D^{*+}/D^0 ratio for $p_T < 40$ GeV/c. Higher statistics are needed to correctly study the tail of the p_T distribution. In PYTHIA8, the D^{*+}/D^0, a vector/pseudoscalar meson ratio, is mainly influenced by spin-counting rules in hadron multiplets, which is in this case for the relative production ratio for primary charm meson governed by the parameter `StringFlav:mesonCvector` (`mesonCvector`), see Tab. 1. In a recent study [58], this value was confirmed to be too low in PYTHIA8 and it was estimated to be 1.5, instead of the default value 0.88. This value improved the D^{*+}/D^0 predictions significantly. This value was obtained however completely arbitrary, hence, as part of the work in this thesis, a tuning is performed of `mesonCvector` in Sec. 6.

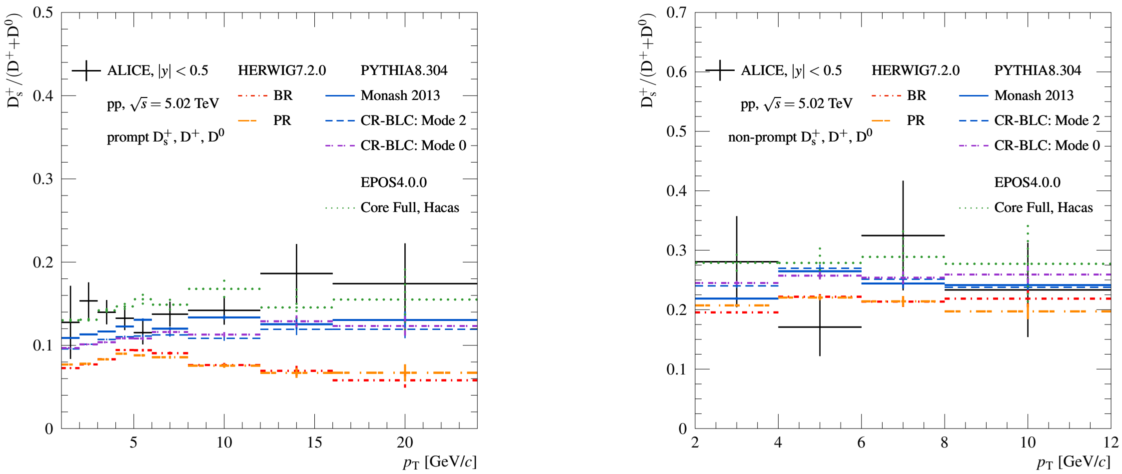

(a) (b)

Figure 20: (a) prompt, (b) non-prompt p_T dependent $D_s^+/(D^0+D^+)$ meson-to-meson ratio in pp collisions $\sqrt{s} = 5.02$ TeV, measured at $|y| < 0.5$ by the ALICE experiment [33], compared with Monte Carlo models.

In Fig. 20, it is observed that both tunes in HERWIG7 generally underestimate the prompt $D_s^+/(D^0+D^+)$ and do not follow the trend of experimental measurement, especially at higher p_T. The parameter controlling the mass distribution of clusters containing a charm quark is `PSplitCharm`. In both tunes, this parameter is set to the default value, thus resulting in similar cluster mass distributions. Only after colour reconnection, the contribution in the high-mass region of the distribution mainly comes from mesonic clusters, hence we would expect a higher non-prompt production rate for different D-meson species from heavier cluster decays, which is observed for lower p_T. The general flat trend of the measurement of non-prompt $D_s^+/(D^0+D^+)$ is generally followed by both HERWIG7 tunes. In Fig. 21, only the BR model in HERWIG7 is compared with the measurements, because of the similar control of mesonic cluster fission and decay in both models. We observe that BR follows the flat trend in D^+/D^0, and describes the data within uncertainties. Similarly, BR follows the increasing trend seen in the measurements for $p_T < 8$ GeV/c in the D^{*+}/D^0 ratio.

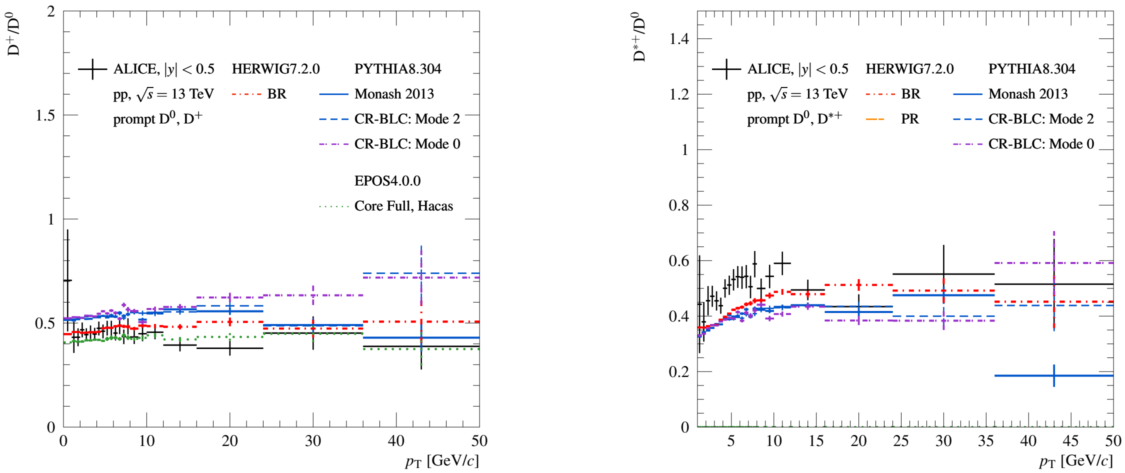

(a) (b)

Figure 21: Prompt p_{T} dependent (a) $\mathrm{D^+/D^0}$ meson-to-meson ratio, (b) $\mathrm{D^{*+}/D^0}$ meson-to-meson ratio, both measured at $|y| < 0.5$ by the ALICE experiment at $\sqrt{s} = 13$ TeV [33, 37], compared with Monte Carlo models.

In EPOS4, by enabling hadronic rescattering and the full core/corona procedure, we observe all meson-meson ratios are described within uncertainties. By default, EPOS4 does not record $\mathrm{D^{*+}}$ resonances because of the short lifetime, hence $\mathrm{D^{*+}}$ comparisons are not included. In Fig. 20, we observe that EPOS4 generally follows the trend in both non-prompt and prompt $\mathrm{D_s^+/(D^0 + D^+)}$ over the full p_{T} range.
As mentioned in Sec. 3.3, the target and projectile remnants are left off-shell and thus will eventually contribute to particle production at large rapidity as part of the corona. For minimum bias collisions at midrapidity (typically described by two pomerons on average), the main contribution to the total of prehadrons comes from core prehadrons [74]. After the core hadronises, the effective mass for a two-pomeron system is relatively small [74], but there is enough phase space to produce D-meson, as observed. The constrained phase space would only be a problem in producing heavy baryons, which are overall underestimated by EPOS4 with the core/corona mechanism as we will see next. After the hadronisation of the core, interactions between the corona and core hadrons are enabled. The fraction of corona hadrons is however relatively small for heavy particles with low $p_{\mathrm{T}} < 3$ GeV/c [74] (see also Eq. 3.6), thus we do not observe a large effect with hadronic rescattering enabled in this region. For clarity, we have left out the comparison with only the core/corona procedure enabled. In general, we have observed that re-scattering makes the D-meson spectra harder since we also include the corona particles that directly come from hard scattering. The charm quarks in EPOS4 are exclusively produced in the parton ladder, and not during the kinky string breaking or in the core plasma. Therefore, it would be interesting to study the multiplicity dependence of D-meson production with EPOS4 and its effect on the saturation scales, with and without the hydrodynamical evolution of the core.

5.1.2 Baryon-to-meson ratios

In this section, a selection of p_{T} dependent baryon-to-meson ratios measured at $|y| < 0.5$ at $\sqrt{s} = 5.02$ TeV and $\sqrt{s} = 13$ TeV by the ALICE experiment [39, 40, 41] are presented, and compared with different Monte Carlo models.

In Fig. 22a, the $\Lambda_{\mathrm{c}}^{+}/\mathrm{D}^{0}$ baryon-to-meson ratio measured at $\sqrt{s} = 5.02$ TeV is presented. The PYTHIA8 Monash tune underestimates the measurements in the interval $p_{\mathrm{T}} < 5$ GeV/c by a factor 4-5, and is also not able to describe the p_{T} dependence of the measurements. It shows, however, that both PYTHIA8 QCD-CR tunes generally describe the measurements within uncertainties but overestimate Λ_{c}^{+} production for low-p_{T}, as seen from the $\Lambda_{\mathrm{c}}^{+}/\mathrm{D}^{0}$ and the enhanced Λ_{c}^{+} production cross section in Fig. 34c. The main reason for this enhancement is that most strings in a PYTHIA8 event are close to parallel to the beam [15], connecting low-p_{T} partons produced by the MPIs. This means that the majority of the total production of baryons from junction reconnections comes from two or three dipoles from such strings along the beam direction, resulting in the enhancement of low-p_{T} baryons. A similar p_{T} dependence of $\Xi_{\mathrm{c}}/\mathrm{D}^{0}$, see Fig. 23, can be observed, however the $\Xi_{\mathrm{c}}/\mathrm{D}^{0}$ ratio is generally lower. This strongly indicates that fragmentation functions among baryons differ significantly.

The PYTHIA8 Monash Tune significantly underestimates the $\Xi_{\mathrm{c}}/\mathrm{D}^{0}$ ratio, since the production of Ξ_{c} baryons is largely underestimated, while the production cross section of prompt D^{0} is described within uncertainties. Both QCD-CR tunes predict a similar magnitude and p_{T} dependence of $\Xi_{\mathrm{c}}/\mathrm{D}^{0}$ ratios. The enhancement of Ξ_{c} production at low-p_{T} is less visible for the strange baryon-to-meson ratios $\Xi_{\mathrm{c}}^{0}/\mathrm{D}^{0}$, $\Xi_{\mathrm{c}}^{+}/\mathrm{D}^{0}$, but it is still reflected in a small increase for low-p_{T}. This can also be seen in the p_{T} distributions of Ξ_{c} in figures 34a and 34b. However, the enhanced baryon production from junctions is insufficient to describe Ξ_{c} production rates. so an additional strangeness-enhancement mechanism is needed. This is already implemented in PYTHIA8, called Rope Hadronization [101, 102], where overlapping strings give an increase in the string tension κ [15], which increases the probability of strange quarks in the string breakups. However, for this thesis, further discussion of QCD-CR parameters for strangeness enhancement or Rope hadronisation will not be the main target. Some preliminary results can be found in [15].

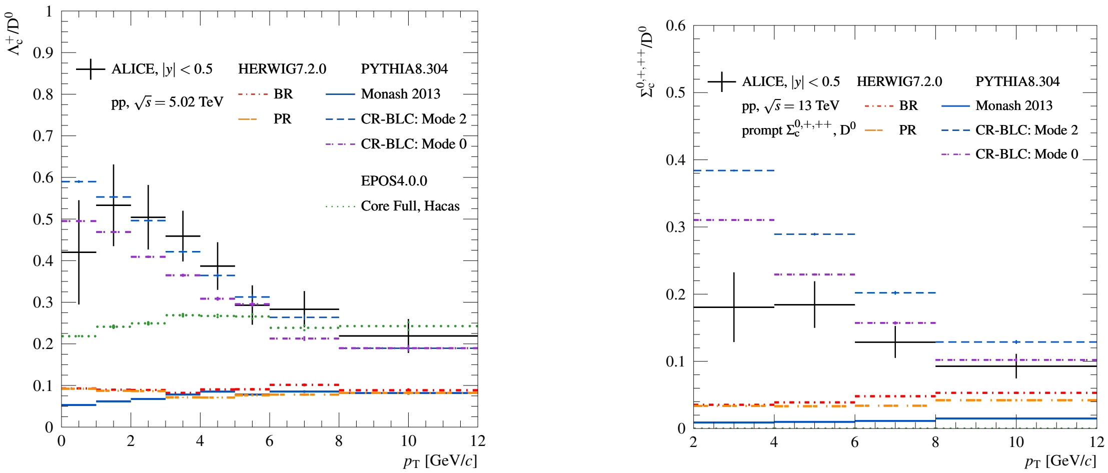

(a) (b)

Figure 22: (a) Λ_c^+/D^0 baryon-to-meson ratio in pp collisions $\sqrt{s} = 5.02$ TeV, (b) $\Sigma_c^{0,+,++}/D^0$ baryon-to-meson ratio in pp collisions at $\sqrt{s} = 13$ TeV, measured at $|y| < 0.5$ by the ALICE experiment [39, 40], compared with Monte Carlo models.

It is clear from figures 22b and 34d that both PYTHIA8 QCD-CR tunes largely overestimate the production of $\Sigma_c^{0,++}(2455)$ baryons, hence overestimating the $\Sigma_c^{0,+,++}(2455)/D^0$ ratio and the Λ_c feed-down from Σ_c. However, generally the tunes follow the trend of the measurements. The parameter mainly influencing the production rate of Σ_c baryons is `StringFlav:probQQ1toQQ0join`, see Tab. 1. After the junction formation between dipoles, the colour strings will again undergo string breaking. Of the three junction legs the two lowest energy legs are fragmented first, where a diquark is formed by combining the flavour and momenta of the two partons closest to the junction point left on the two legs. The spin assignment of the junction diquark is handled by the parameter mentioned above, via a suppression of spin-1 diquark formation relative to spin-0. The suppression factor is additional to the enhancement to the factor 3 by simply counting the number of spin states. The production of spin-3/2 baryons can be directly controlled by the production of spin-1 diquarks. The parameter has four components that control the suppression factor given the heaviest quark flavour present is respectively $u/d, s, c, b$ [58]. The chosen values for this parameter in PYTHIA8 QCD-CR tunes were not tuned to any particular data, and thus arbitrarily set to be equal and relatively low. By increasing the probability for a diquark to be in a spin-1 instead of a spin-0 state, the formation of excited spin-3/2 Σ_c and Λ_c baryons are favored over Σ_c baryons in the subsequent fragmentation of the largest leg. These spin-3/2 excited states decay favorably to Λ_c instead of Σ_c, which would result in a lower production rate for Σ_c [5].

In contrast, the values of the `StringFlav:probQQ1toQQ0join` parameter are higher in Monash. In combination with the absence of QCD CR mechanisms, the $\Sigma_c^{0,+,++}(2455)/D^0$ is significantly underestimated. In recent studies [15, 58], the values for `StringFlav:probQQ1toQQ0join` in the Monash Tune were used in QCD-CR Mode 2, which significantly improved the agreement between the model and the experimental measurements. Since these values are also chosen arbitrarily, a tuning of this parameter, specifically for the charm entry, is done in Sec. 6.

In figures 34a and 34b, both PR and BR models in HERWIG7 significantly underestimate Ξ_c production, although generally a similar trend between measurements and predictions is presented. One can also observe an increase in production with the BR model of Ξ_c for the full p_T range with respect to the PR model. In both PR and BR models, we have allowed non-perturbative gluon splitting into strange quarks with a given probability `SplitPwtSquark`, and to allow the possibility to select a strange quark during cluster fission `PwtSquark`. Only due to the higher probability of baryonic colour reconnection in BR, we would expect a larger fraction of strange quarks to be part of baryonic clusters, hence enhancing Ξ_c production over the full p_T range.

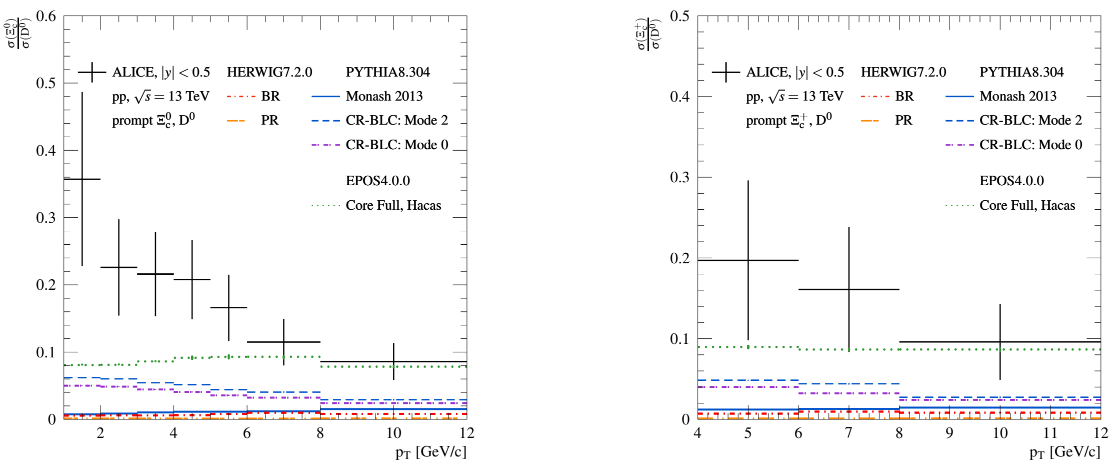

(a) (b)

Figure 23: (a) Ξ_c^0/D^0 (b) Ξ_c^+/D^0 baryon-to-meson ratios in pp collisions at $\sqrt{s} = 13$ TeV measured at $|y| < 0.5$ by the ALICE experiment [41], compared to Monte Carlo models.

In figures 34c and 34d, a smaller increase is shown in the production of Λ_c and Σ_c baryons at the higher p_T end of the spectrum with BR compared to the PR model. This can also be explained by the larger baryonic reconnection probability, which reduces the number of high-multiplicity events and shifts them towards lower multiplicities. One of the consequences of the BR model is that high-multiplicity events yield a large fraction of baryonic reconnections. Due to the highly restricted phase space for baryon production from baryonic clusters, fewer particles are produced than with mesonic clusters of similar invariant mass [66]. This restriction in baryon production leads to a lower charged particle multiplicity. As a result, there is an increased production of heavy particles with higher p_T. Conversely, this increase is not observed in prompt D-meson production, see figures 18a and 33d, where both PR and BR models describe prompt D^0 and D^+ production within uncertainties. Additionally, by directly comparing the cluster masses after colour reconnection, it is shown that the contribution in the high-mass region mainly comes from mesonic clusters, and large baryonic clusters are still highly suppressed [66]. These smaller baryonic clusters lead to fewer heavy particles due to the restricted phase space in the cluster decay stage. Consequently, this results in a large underestimation in the ratios of Ξ_c, Λ_c, Σ_c baryons with respect to D^0, see figures 22 and 23.

By default, EPOS4 does not record Σ_c baryons because of the short lifetime, hence Σ_c comparisons are not included in our study. In Fig. 22a, we observe a relatively flat p_T dependence for the Λ_c^+/D^0 ratio. This p_T independence is also observed in Ξ_c/D^0 ratios. In figures 34a and 34b we see that EPOS4 (with full core/corona and hadronic rescattering), shows the best predictions for the Ξ_c. In general, the p_T trend of the measurements is followed, and the data is described within uncertainties for $p_T > 6$ GeV/c. As already mentioned, we would expect a large contribution of corona prehadrons to the total production at higher p_T. It is possible that in the breaking of these high-p_T kinky strings more strange quarks with high-p_T are produced at the kinks. Hence we would observe a better agreement for high-p_T Ξ_c spectra. We see a similar p_T hardening in Λ_c baryons in Fig. 34c. Still, for low-p_T, EPOS4 generally underestimates charmed baryon production, since fragmentation is the main source of hadronisation of heavy quarks in EPOS4. By adding coalescence mechanisms, where charm quarks can interact with lighter quarks in the core, we would expect a larger production for low-p_T baryons. This is for example implemented in EPOS4HQ, which shows better agreement for baryon-to-meson ratios [81].

5.1.3 Baryon-to-baryon ratios

In this section, a selection of p_T-dependent baryon-to-baryon ratios in pp collisions measured at $|y| < 0.5$ at $\sqrt{s} = 13$ TeV by the ALICE experiment [40, 41] are presented, and compared with different Monte Carlo models.

In Fig. 24a, the $\Lambda_c^+(\leftarrow \Sigma_c^{0,++}) \times 3/2 \ / \ \Lambda_c^+$ ratio is presented. It is clear that both PYTHIA QCD-CR models generally describe the downward trend of the measurements, but significantly overestimate the feed-down of Λ_c from the ground state $\Sigma_c(2455)$ baryons, hence overestimating the ratio to total Λ_c production. As mentioned, this excess in feed-down is due to an overestimation of Σ_c baryons, which primarily decay to Λ_c. In Fig. 34e, we assume symmetrical feed-down to Λ_c^+ from the three different Σ_c isospin states, hence the factor 3/2. By increasing the probability of spin-1 diquark formation in junction fragmentation, it would produce more excited spin-3/2 Σ_c baryons, instead of spin-1/2 $\Sigma_c(2455)$, hence reducing the Λ_c^+ feed-down from $\Sigma_c(2455)$ baryons. This probability increase is implemented in the PYTHIA Monash, see Tab. 1, hence this ratio is significantly lower over the full p_T range.

All PYTHIA8 tunes significantly underestimate the prompt Ξ_c^0/Λ_c^+ ratio in Fig. 24b, since the Ξ_c production is underestimated by the tunes. We also observe that the downward trend is not well described by the tunes, but a small increasing trend is observed. We see this underestimation also for the PYTHIA QCD-CR models in the $\Xi_c^{0,+}/\Sigma_c^{0,+,++}$ ratio in Fig. 24c, mainly since $\Sigma_c^{0,+,++}$ is generally overestimated in these models. Also, the general trend is not well predicted by the PYTHIA QCD-CR models. By decreasing the Σ_c production, we would only slightly enhance the $\Xi_c^{0,+}/\Sigma_c^{0,+,++}$ prediction, since $\Xi_c^{0,+}$ is still generally underestimated. We would need an additional strangeness enhancement mechanism in the QCD-CR models to describe this ratio accurately. Since both Σ_c and Ξ_c production are largely underestimated in PYTHIA Monash, we observe that Monash describes the $\Xi_c^{0,+}/\Sigma_c^{0,+,++}$ ratio within uncertainties. Naturally, this observation yields nothing physical, since both primary spectra are still underestimated.

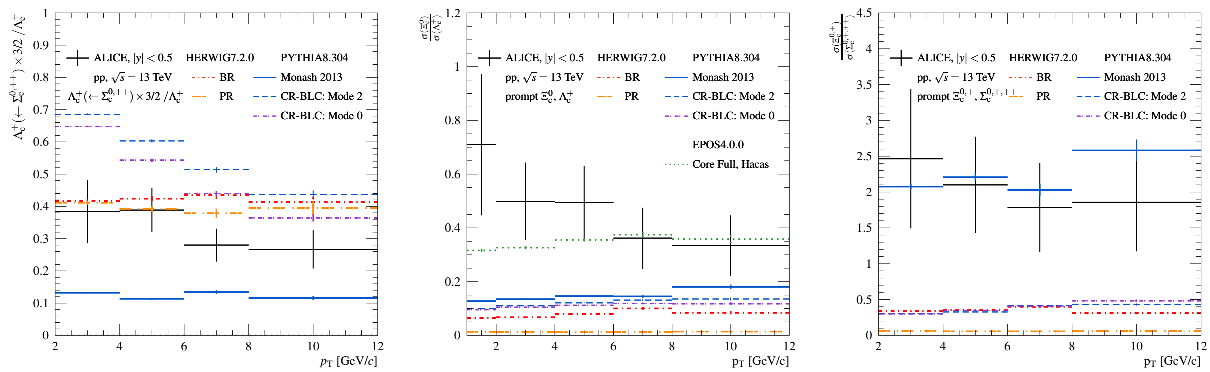

(a) (b) (c)

Figure 24: p_T-differential per unit rapidity (a) $\Lambda_c^+(\leftarrow \Sigma_c^{0,++}) \times 3/2$ / Λ_c^+ (b) Ξ_c^0/Λ_c^+ and (c) $\Xi_c^{0,+}/\Sigma_c^{0,+,++}$ baryon-to-baryon ratios in pp collisions at $\sqrt{s} = 13$ TeV measured at $|y| < 0.5$ by the ALICE experiment [40, 41], compared to Monte Carlo models.

Both PR and BR models in HERWIG7 describe the feed-down fraction of Λ_c from Σ_c within uncertainties for $p_T < 6$ GeV/c. They generally show a flat p_T trend, hence overestimating the feed-down fraction for $p_T > 6$ GeV/c. This trend is however expected due to a similar decreasing trend seen in the Λ_c feed-down and Λ_c production cross sections. Also the Σ_c primarily decays to Λ_c baryons, thus we expect the Λ_c production to follow the feed-down of Λ_c from Σ_c in clustering decay models. This flat trend is seen in both BR and PR models, so the feed-down fraction of Λ_c is handled similarly in the cluster decay mechanism. For the Ξ_c^0/Λ_c^+ ratio, we observe a slight increase in the BR model compared to the PR. Both models however significantly underestimate Ξ_c^0/Λ_c^+. Due to the higher probability of baryonic colour reconnection in BR and enhanced strangeness in both models, we would expect a larger fraction of strange quarks to be part of baryonic clusters, hence increasing Ξ_c production over the full p_T range. The Λ_c enhancement is expected to be smaller since only baryonic clustering would enhance the production. For this reason, an increase in Ξ_c^0/Λ_c^+ is expected for BR compared to PR. Similar behavior is observed for the $\Xi_c^{0,+}/\Sigma_c^{0,+,++}$ ratio, where also both models significantly underestimate this ratio.

In Fig. 24b, we observe a relatively flat p_T dependence for the Ξ_c/Λ_c^+ ratio in EPOS4. For $p_T > 6$ GeV/c, EPOS4 describes the measurements within uncertainty. However, for low-p_T, the baryon-to-baryon ratio is generally underestimated. This is mainly because the main source for heavy quark hadronisation in EPOS4 is fragmentation. By adding coalescence mechanisms, where charm quarks can interact with lighter quarks in the core, we would expect a larger production for low-p_T charmed baryons. This would potentially also enhance strangeness in heavy baryons, since low-p_T strange quarks that are created in the initial parton ladders are more likely to recombine with charm quarks. Moreover, the rescattering of heavy baryon-antibaryon pairs has been enabled, for which we also observe a small decrease in the production of low-p_{T} baryons.

5.2 Charmed hadrons production study in heavy-ion collisions

In this section, a subset of p_{T}-differential production cross sections and baryon-to-meson ratios in p–Pb and Pb–Pb collisions measured at $\sqrt{s_{\mathrm{NN}}} = 5.02$ TeV by the ALICE experiment are presented, and compared with different Monte Carlo models. Moreover, we use the pp references from the different models in Fig. 33 to predict the R_{pPb} and R_{AA} observables in PYTHIA8. For Pb–Pb collisions, we will mainly present prediction on central (0-10%) collisions.

It should be noted that, on a conceptual level, there are differences between pp events with the MPI model implemented in PYTHIA8 and heavy-ion events generated with PYTHIA8 using Angantyr. The MPI-based colour reconnection is only applied at the level of individual nucleon-nucleon collisions [12]. The current MPI model in PYTHIA8 does not include a dependence on the impact parameter but assumes that the soft MPIs will have a larger spatial spread, and thus will reconnect more easily with harder systems. This is a reasonable assumption for pp collisions since all systems are confined to the transverse size of an individual nucleon. Naturally, this is not applicable in heavy-ion collisions. The next step would be to implement a CR model that accommodates partons from different sub-collisions (resembling collective behavior) and is dependent on spatial parameters. This has already been implemented as a global reconnection tune in [14]. In this part, we will rather demonstrate the behavior of heavy-ion collisions when we consider no parton-level QGP-like interactions (PYTHIA8 with Angantyr). For future research, this can be compared to predictions when we do consider QGP-like interactions, for example with EPOS4.

In Fig. 25, the Λ_{c}^{+} production cross section and $\Lambda_{\mathrm{c}}^{+}/\mathrm{D}^{0}$ baryon-to-meson ratio in p–Pb collisions are presented respectively. Clearly, PYTHIA8 Monash with Angantyr significantly underestimates the production cross-section of prompt Λ_{c}^{+} baryons. In Fig. 35, we left out the prediction of the production cross sections of D-mesons in p–Pb collisions for clarity reasons, but a similar prediction has been observed as in Pb–Pb collisions. Each tested PYTHIA8 tune with Angantyr, especially Monash, predicts the p_{T}-differential cross section within uncertainties, hinting that there is no need for collective-like effects to predict the measurements of D-mesons production in heavy-ion collisions. Moreover, we observe that the production of Λ_{c}^{+} is also slightly underestimated by the PYTHIA8 QCD-CR tunes with Angantyr. We observe however a larger production than Monash, hinting that baryon enhancement is also present in the hadronisation of individual sub-collisions due to the formation of junction topologies within sub-collisions. For this reason, we see that the trend in the $\Lambda_{\mathrm{c}}^{+}/\mathrm{D}^{0}$ ratio measurement is generally described by QCD-CR tunes with Angantyr, especially for $p_{\mathrm{T}} > 3$ GeV/c. However, the magnitude of the measurement is still slightly underestimated (note the linear scale). The Monash tune with Angantyr is not able to predict the general trend and the magnitude of the $\Lambda_{\mathrm{c}}^{+}/\mathrm{D}^{0}$ ratio. Therefore, it would be interesting to study the baryon-to-meson ratios with a spatial color reconnection model including BLC-CR effects between different sub-collisions. This model will also describe potentially better the low-$p_{\mathrm{T}} < 3$ GeV/c region since this is overestimated by the PYTHIA8 QCD-CR tunes with

Angantyr. This model would however need to be retuned on pp collisions, this is done in [14].

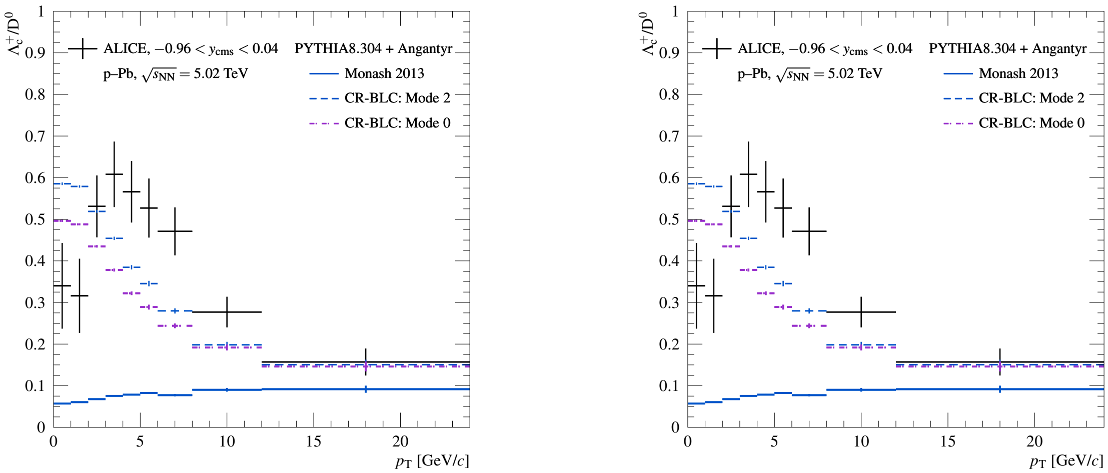

(a) (b)

Figure 25: The p_{T}-differential (a) production cross section of prompt Λ_{c}^{+} per unit rapidity and (b) $\Lambda_{\mathrm{c}}^{+}/\mathrm{D}^{0}$ in p–Pb collisions measured by the ALICE experiment [39] for $-0.96 < y_{\mathrm{cms}} < 0.04$ at $\sqrt{s_{\mathrm{NN}}} = 5.02$ TeV, compared to Monte Carlo models.

In Fig. 26, a similar baryon enhancement is observed in central Pb–Pb collisions in QCD-CR tunes compared to Monash with Angantyr. This is again purely because of the formation of beyond-leading colour topologies within the nucleon-nucleon collisions, similar to pp collisions, and not due to collective effects. This enhancement is mainly observed for the low-p_{T} region since the color strings involved in the formation of junctions will come from low-p_{T} partons produced by the MPIs. However, the $\Lambda_{\mathrm{c}}^{+}/\mathrm{D}^{0}$ is still largely underestimated by QCD-CR models for intermediate 5 GeV/$c < p_{\mathrm{T}} <$ 12 GeV/c. This hints towards collective effects, where due to coalescence, a larger Λ_{c}^{+} production is observed.

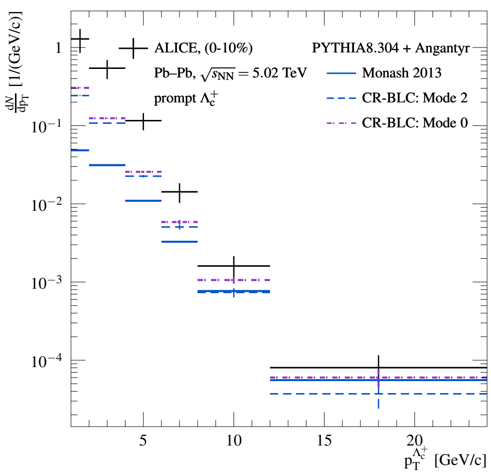

(a)

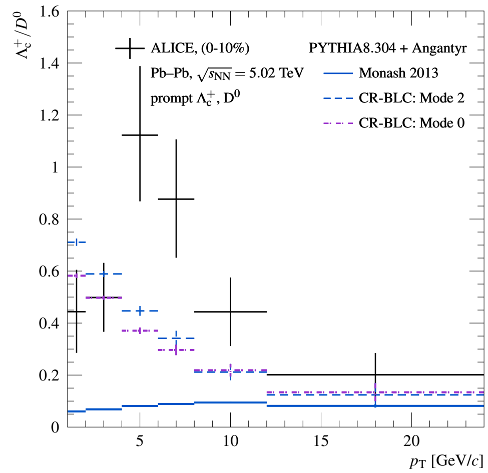

(b)

Figure 26: The p_{T}-differential (a) production cross section of prompt Λ_{c}^{+} and (b) $\Lambda_{\mathrm{c}}^{+}/\mathrm{D}^0$ in central Pb–Pb collisions (0-10%) measured by the ALICE experiment [44] at $\sqrt{s_{\mathrm{NN}}} = 5.02$ TeV, compared to Monte Carlo models.

In Fig. 27, the R_{pPb} and R_{AA} in central collisions (0-10%) of prompt Λ_{c}^{+} are presented respectively. All PYTHIA8 tunes with Angantyr do not follow the trend of the measurements and only describe the data within uncertainties for high-p_{T} in Pb–Pb collisions, especially Monash. This suggests that no QGP-like modification is necessary for high-p_{T} partons to describe R_{AA} with PYTHIA8 with Angantyr. A similar flat trend is observed in the prediction for the average R_{AA} of D^0, D^+ and D^{*+} in both central and peripheral Pb–Pb collisions. Again, Monash describes the measurements within uncertainties for higher p_{T}. For D-mesons, especially in peripheral Pb–Pb collisions, the additional QCD-CR parameters worsen the predictions.

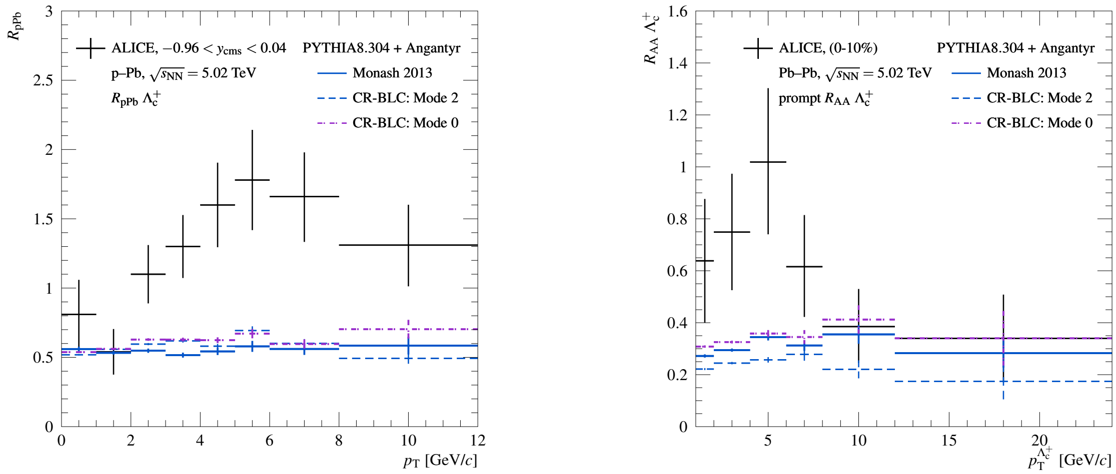

Figure 27: The p_{T}-differential (a) R_{pPb} prompt Λ_c^+ measured for $-0.96 < y_{\mathrm{cms}} < 0.04$ in p–Pb collisions by the ALICE experiment [39], and (b) R_{AA} of prompt Λ_c^+ in central Pb–Pb collisions (0-10%) measured by the ALICE experiment [44]. Both quantities are measured at $\sqrt{s_{\mathrm{NN}}} = 5.02$ TeV, and compared to Monte Carlo models.

Angantyr is based on the wounded nucleon model, where nuclear shadowing effects are included for the treatment of secondary wounded nucleons [59]. Consequently, not all possible nucleon-nucleon interactions from the Glauber calculation are realized in the generation of the final state, thus it has no correct N_{coll} scaling built in. This means that in general R_{pPb} and $R_{\mathrm{AA}} < 1$ since we simply scaled by N_{coll} based on Glauber calculations from ALICE. Interestingly, nuclear shadowing effects are present over the full p_{T} spectrum. By looking at factorization we would however expect at large values of p_{T}, that N_{coll} is obeyed [13], only implementing this separation scale between soft and hard processes is generally difficult.

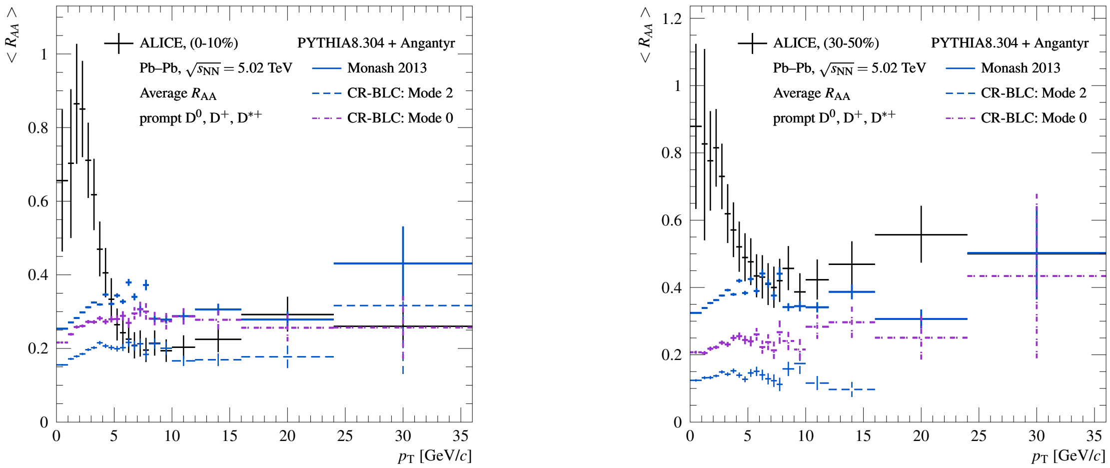

(a) (b)

Figure 28: The p_T-differential average R_{AA} of D^0, D^+ and D^{*+} in Pb–Pb collisions for (a) 0-10% and (b) 30-50% centrality bins measured by the ALICE experiment [35]. Both quantities are measured at $\sqrt{s_{NN}} = 5.02$ TeV, and compared to Monte Carlo models.

Summary of results

In this section, we have performed an important review of some of the available state-of-the-art Monte Carlo models and applied these to recent ALICE results. Generally, D-meson production in pp collisions at $\sqrt{s} = 5.02$ TeV and $\sqrt{s} = 13$ TeV at mid rapidity is described well by all three tested PYTHIA8 tunes and EPOS4, although ratios between prompt D-mesons including strangeness are best described by EPOS4, with enabled hadronic rescattering and full core/corona procedure. Both PR and BR in HERWIG7 generally underestimates prompt D_s^+ mesons, hence not describing well the $D_s^+/(D^0 + D^+)$ meson-to-meson ratio.
Both PYTHIA8 QCD-CR tunes Mode 0 and Mode 2 describe the Λ_c^+/D^0 baryon-to-meson ratio in pp collisions within uncertainties due to the formation of junction topologies enhancing baryon production. Both QCD-CR tunes overestimate Σ_c production. Only MPI-based color reconnection is implemented in Monash and HERWIG7 (both BR and PR), hence they underestimate Λ_c, Σ_c and Ξ_c baryon production significantly. Some increase in baryon production in BR is observed due to the formation of baryonic clusters. EPOS4 with hadronic rescattering and full core/corona procedure also underestimates baryon production but is able to describe the measurements for higher p_T within uncertainties.
In pp collisions, both Mode 0 and Mode 2 overestimate the feed-down fraction $\Lambda_c^+(\leftarrow \Sigma_c^{0,++}) \times 3/2 \;/\; \Lambda_c^+$. PR and BR tunes in HERWIG7 both describe this measurement within uncertainties. Only EPOS4, enabled with hadronic rescattering and full core/corona procedure, describes the Ξ_c^0/Λ_c^+ for high-p_T. Moreover, only the PTYHIA8 Monash tune describes $\Xi_c^{0,+}/\Sigma_c^{0,+,++}$, which is mainly accidental.
In heavy-ion collisions, enhancement of Λ_c baryons production is also observed by allowing the formation of junction topologies in individual sub-collisions. Since the Angantyr model in PYTHIA8 is based on the wounded nucleon model, the nuclear modification factors R_{pPb} and R_{AA} are not well described.

6 Tuning of PYTHIA8 CR Mode 2

6.1 Parameter Based Tuning

The main methods for generator tuning with RIVET are the simple *by-eye* method or a brute-force method by trying a set of parameters in the parameter space. However, both methods are extremely expensive and naturally not optimal for high-dimensional parameter spaces.

In this thesis, we will use the method to parameterize the generator [105]. We expect the global fit function to the data to be complicated in itself, hence it will not be parameterisable. For this reason, we fit a polynomial or rational function to the *response* of the generator, MC_b, of each observable bin b to the changes in the $n-$dimensional parameter vector $\mathbf{p} = (p_1, \cdots, p_n)$. After this polynomial parameterization is built, we need to construct a goodness-of-fit measure and minimize it. The output of the minimization is a parameter vector, $\mathbf{p}_{\text{tune}}$, which in principle should predict the best description of the data the generator can simulate. Since the distributions we study will have a different weight on the total goodness-of-fit measure (for example different number of bins), we want to include per-observable weighting $w_{\mathcal{O}}$ for each observable $\mathcal{O}$ in the observable space $S_{\mathcal{O}}$, in our heuristic goodness-of-fit measure χ^2 [105]:

$$\chi^2(\mathbf{p}) = \sum_{\mathcal{O}\in S_{\mathcal{O}}} w_{\mathcal{O}} \sum_{b\in\mathcal{O}} \frac{(t_b(\mathbf{p}) - \mathcal{R}_b)^2}{\Delta t_b(\mathbf{p}) + \Delta_b^2}, \tag{6.1}$$

where $\mathcal{R}_b$ is the reference value for bin b, and Δ_b is the total uncertainty of the reference for bin b. The goal is to find a parameter vector $\mathbf{p}_{\text{tune}}$ which will predict the bin value output of the generator t_b and the error estimation per bin Δt_b that globally (over multiple observables $\mathcal{O} \in S_{\mathcal{O}}$) minimizes Eq. 6.1.

6.2 Tuning Kinematics

6.2.1 Tuning Parameters

As mentioned in Sec. 5, the overestimation of $\Sigma_c^{0,++}(2455)$ baryon production mainly comes from the third entry of the parameter `StringFlav:probQQ1toQQ0join`, which we will call joinC, and the value joinC = 0.0275 in CR Mode 2 is too low (see Tab. 1). The spin assignment of the junction diquark is handled by joinC via suppression of spin-1 diquark formation relative to spin-0 states. Consequently, this parameter can directly control the production of spin-3/2 baryons containing a charm quark. By increasing the probability for a diquark to be in a spin-1 instead of a spin-0 state, the formation of excited spin-3/2 Σ_c^* and Λ_c^* baryons are favored over Σ_c baryons in the subsequent fragmentation of the largest leg. These spin-3/2 excited states decay favorably to Λ_c instead of Σ_c [5], resulting in a lower production rate for $\Sigma_c(2455)$ baryons [58]. We expect this parameter to be much larger. Also, we expect that increasing the value of this parameter would decrease the Λ_c^+ feed-down from $\Sigma_c(2455)$ baryons, hence more accurately describing the measurements. Considering the changes in the two observables mentioned above, we expect no direct alteration in the total production of Λ_c^+ baryons. Hence, we expect a large improvement in the generally overestimated

$\Lambda_c^+(\leftarrow \Sigma_c^{0,++}) \times 3/2 \,/\, \Lambda_c^+$ ratio, see Fig. 24a.

In Sec. 5, it was also observed that CR Mode 2 generally underestimates the D^{*+}/D^0 and D_s^+/D^+ ratios, and overestimates the D^+/D^0 ratio. In CR Mode 2 vector/pseudoscalar meson ratios are mainly influenced by spin-counting rules in hadron multiplets, which is for the relative production ratio for primary charm meson governed by the parameter `StringFlav:mesonCvector` (= 0.88 in CR Mode 2), which we call mCv. In a recent study [58], this value was studied to be too low in PYTHIA8, but a tuned value was still absent. By increasing the value of mCv we expect an increase in vector $D^{*+}(2010)$ meson production, and hence a small increase in D^0 production, since D^{*+} decays favorably to D^0 [5]. Consequently, we would decrease the general overestimated D^+/D^0 ratio by the default CR Mode 2.

6.2.2 Tuning Datasets

For the tuning of the parameters mCv and joinC in PYTHIA8 CR Mode 2, we exclusively use data by the ALICE experiment, as discussed in Sec. 5, since this is the most relevant source of information of charm hadron production at low p_T. The following datasets in pp collisions are used for the tuning:

- prompt D^0, D^{*+}, D^+ and D_s^+ p_T-differential cross section spectra at $\sqrt{s} = 13$ TeV for $p_T < 24$ GeV/c [37].
- prompt $\Sigma_c^{0,+,++}$ p_T-differential cross section spectra at $\sqrt{s} = 13$ TeV for $p_T < 12$ GeV/c [40].
- prompt $\Lambda_c^+(\leftarrow \Sigma_c^{0,+,++})$ p_T-differential cross section spectra at $\sqrt{s} = 13$ TeV for $p_T < 12$ GeV/c [40].

The data are publicly available in the form of histograms of cross-sections. Note that we also include the conjugates of all the particle spectra mentioned above. Several hadron-to-hadron ratios, discussed in Sec 5, would be directly influenced by changes in the parameters. For the parameter tuning, we will solely focus on the primary particle spectra mentioned above, because using ratios would yield non-physical results since they derive from primary spectra. As mentioned, we will not perform parameter tuning or study parameters related to strangeness enhancement.

6.2.3 Tuning Methods

In the first step, a range for optimal value for mCv was estimated by tuning on D-meson spectra - leaving the joinC on its default value. Similarly, in the second step, the optimized value range for joinC was estimated on Σ_c-baryon spectra - while fixing the default mCv CR Mode 2 flavour parameter. For each parameter point on the border of the (mCv, joinC) parameter space 100 million pp collisions were generated while keeping `SoftQCD:all=on`. After this, 100 million pp collisions at $\sqrt{s} = 13$ TeV were generated per parameter point in the estimated optimal parameter space (mCv, joinC) using grid sampling. The estimated optimal range for (mCv, joinC) came out to be $[1.3 - 1.6]$ and $[0.66 - 1.0]$ respectively. We found that the parameters mCv and joinC are decoupled well, so we would not expect large differences in tuned values, compared to tuning the values separately. We used the RIVET routines ALICE_2023_I2697877 and ALICE_2021_I1868463 for the analysis of the spectra, see Sec. 4.2. With each run, we obtain a set of histograms for each point in the optimal parameter space. For the generation of data for tuning joinC, we used the default Monash tune values for the other three entries of StringFlav:probQQ1toQQjoin, see Tab. 1, instead of the CR Mode 2 values. These entries are however still arbitrary guesses and need to be tuned and studied in further detail [58]. The Monash Tune values are however following the quark mass, which is to be expected. The probability of spin-1 or spin-0 diquark reconnection should be mass-dependent since the mass splitting between the spin-0 and spin-1 state should be smaller when heavier quarks are involved [15].

Next, we could define a goodness-of-fit measure and numerically find a best-fit point that minimizes the measure, which would however be extremely expensive [104]. Instead, we used a surrogate model that allows us to predict the simulation outcome at any point in the parameter space. For this, we used the Apprentice toolkit for event generator tuning [103], which builds the surrogate model and calculates the minimization of a goodness-of-fit measure. We explored different types of surrogate models but found that polynomials with order $n = 3$ worked well. Apprentice uses in principle rational function approximation (quotients of polynomials p, q, i.e. $r(\mathbf{p}) = p(\mathbf{p})/q(\mathbf{p})$), so in our method we set $n = 3$ for polynomial p and $n = 0$ for polynomial q, mainly to avoid having singularities in the bin approximations. Furthermore, the errors on the generated data points are approximated with quadratic polynomials (order of p, q is $2, 0$ respectively). We used the full simulation results as the input for the surrogate model, excluding the $p_{\mathrm{T}} > 24$ GeV/c bins due to low statistics, hence resulting in unreliable tuning. We generated data with 20 distributed points (by using grid sampling) in the specified range for mCv and joinC to over-sample the parameter space. We would at minimum need 10 polynomial coefficients for polynomials of third order for approximating two parameters [105].
Apprentice allows to bias the goodness-of-fit measure from Eq. 6.1, using an individual weighting mechanisms for bins and histograms [103]. Since the datasets under consideration have large differences in the number of bins, see for example figures 33d and 34d, we decided on a democratic weighting of the histograms, such that each of the six histograms are normalized according to the number of bins. Thus, for a given particle spectrum from Sec. 6.2.2, the weighting w_j of the set j with number of bins N_{bins} can be calculated as $w_j = (N_{\mathrm{bins,j}})^{-1} \cdot a_{\mathrm{norm}}$, with $a_{\mathrm{norm}} = \frac{\sum_i N_{\mathrm{bins,i}}}{\sum_i (N_{\mathrm{bins,i}})^{-1}}$.
Next, we let Apprentice globally minimize the weighted goodness-of-fit measure using the Truncated Newton method (TN) [106]. We set 10^5 randomly selected points as starting points and rerun the minimization 10 times. The output is a best-fit point (mCv, joinC), with a χ^2/NDF, and predicted data including uncertainties given at the best-fit point. For completeness, besides the numerical minimization procedure described above, we use a Bayesian inference technique (BI) that allows for parameter estimation and model selection. The algorithm for sampling the estimated parameter space is based on nested and disjoint multi-dimensional ellipse sampling [107]. Lastly, these spectra are compared to the actual PYTHIA8 output of the simulation with the best-fit point parameters as an input to validate the method.

6.3 Tuning Results and Discussion

The best-fit values for mCv and joinC with the TN method (χ^2/NDF = 2.12) and with the BI technique can be found in Tab. 2. It can immediately be seen that both tuned parameters are significantly larger than the default CR Mode 2, which was to be expected. Furthermore, we observe that the tuned parameters from both minimization methods do not differ significantly.

Parameter	QCD-CR Mode 2 (Default)	Tuned (TN)	Tuned (BI)
mesonCvector	**0.88**	**1.48**	$\mathbf{1.46}^{+0.04}_{-0.04}$
probQQ1toQQ0join	$0.0275, 0.0275, \mathbf{0.0275}, 0.0275$	$0.5, 0.7, \mathbf{0.72}, 1.0$	$0.5, 0.7, \mathbf{0.72}^{+0.02}_{-0.01}, 1.0$

Table 2: Default parameters of CR Mode 2 (left) and Tuned parameters mCv and joinC with the TN method in bold (middle) and with the BI technique (right). Instead of the default parameters in CR Mode 2 for the other entries of `StringFlav:probQQ1toQQjoin`, the default values for the Monash tune were used [58], see Tab. 1.

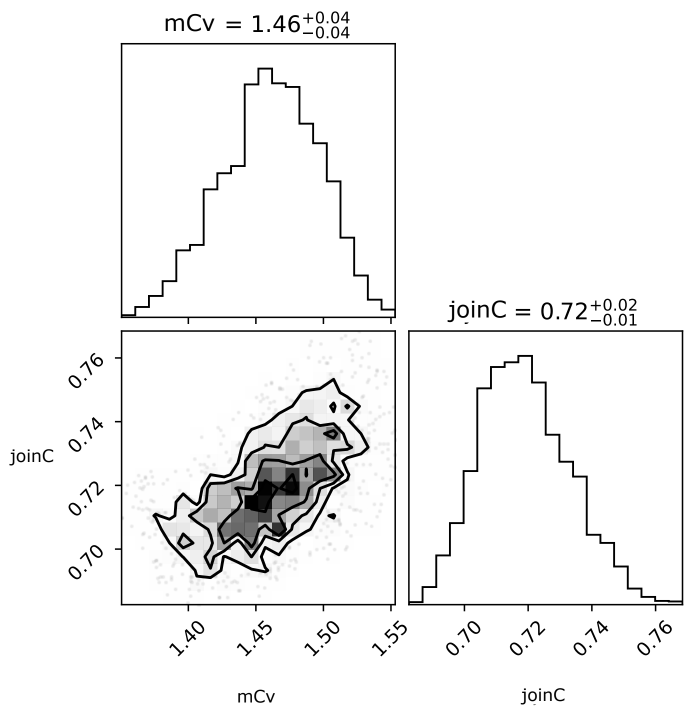

Figure 29: Corner plot of tuned CR Mode 2 parameters obtained with the Bayesian Inference method. The darker shades inside the contours represent the 1-σ level for a 2D density plot. The vertical axes in the 1D histograms represent the probability to be the respective parameter value

The comparison plots of prompt p_{T}-differential production cross sections of D-mesons are presented in Fig. 30. Since both tuning methods resulted in similar parameters, we only present the PYTHIA8 predictions with the tuned parameters using the TN method.

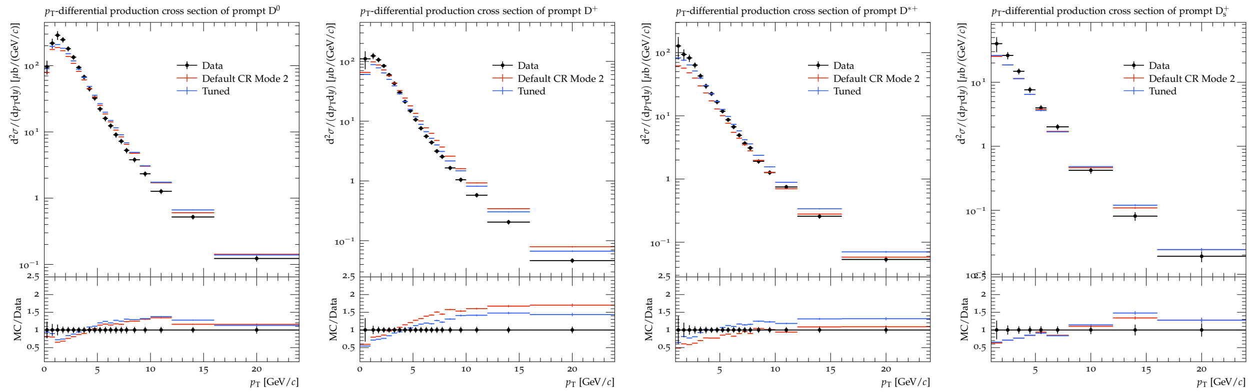

(a) (b) (c) (d)

Figure 30: Prompt D^0 (a), D^+ (b), D^{*+} (c), D_s^+ (d) p_T-differential cross sections, compared with PYTHIA8 CR Mode 2 without (orange) and with our tuned values (blue).

At first glance, the overestimated D^+ production cross section is largely improved. The already well-predicted D^{*+} cross-section production is overestimated by our tuned mCv value. The D^{*+} meson primarily decays to D^0 mesons and charged pions (we also include conjugates in our study), so we see a small increase in D^0 production. Since we also create more charged pions, it would be suitable to include charged pion distributions to validate the obtained tuned values in further studies. With the changes in D-meson spectra, we see a significant improvement in $\mathrm{D}^+/\mathrm{D}^0$, $\mathrm{D}^{*+}/\mathrm{D}^0$, $\mathrm{D}_\mathrm{s}^+/\mathrm{D}^+$ meson ratios in Fig. 31. All the other meson-to-meson- ratios discussed in Sec. 5 are not altered significantly or did not have reference data, hence we did not study these ratios. We would however expect a significant increase in $\mathrm{D}^{*+}/\mathrm{D}^+$ ratio values. Since the D^0 production is slightly increased, the generally overestimated $\Lambda_\mathrm{c}^+/\mathrm{D}^0$ is improved, especially for low p_T.

By further increasing the value of mCv, the D^{*+} production would keep increasing, but a better prediction of D^+ production would be achieved. However, the goodness-of-fit measure in Eq. 6.1 would not be globally minimized in this last case. This gives us a hint that there are potentially additional mechanisms that influence vector- and pseudoscalar charmed meson production which are simply not encompassed by the mCv parameter.

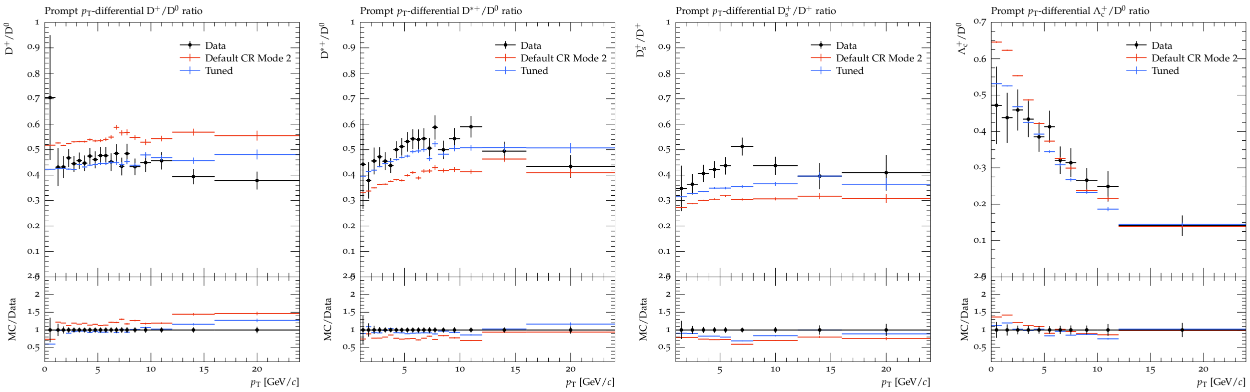

(a) (b) (c) (d)

Figure 31: Prompt $\mathrm{D}^+/\mathrm{D}^0$ (a), $\mathrm{D}^{*+}/\mathrm{D}^0$ (b), $\mathrm{D_s^+}/\mathrm{D}^+$ (c), $\Lambda_\mathrm{c}^+/\mathrm{D}^0$ (d) ratios, compared with PYTHIA8 CR Mode 2 without (orange) and with our tuned values (blue).

The tuning procedure provides slightly different values if we include the highest p_T-bins ($p_\mathrm{T} > 24$ GeV/c) for the D-meson production cross sections. However, for our tune, these bins are excluded due to unpredictable behavior caused by low statistics. The statistical errors on our bin values are relatively small since we generated around 100 million pp events for every point in the estimated optimal parameter space. A possible interesting study, not targeted by this thesis, would be to analyze the effects between the number of events and the approximation of bin errors, with regards to minimizing Eq. 6.1 and hence the tuned parameter values. For the tuned values in Tab. 2 we also trained the bin errors, but it did not affect significantly the resulting tune.

Finally, we compare the default CR Mode 2 tune with and without our tuned parameters for the $\Sigma_c(2455)$ production cross section, its subsequent feed-down to Λ_c^+, and ratios in Fig. 32. We can observe that the tuned value for joinC significantly decreases the $\Sigma_c(2455)$ production cross section and a reduction in the subsequent feed-down to Λ_c^+, leading to a better prediction of the measurements. This behavior is expected as explained in Sec. 6.2.1. Furthermore, we see a significant improvement in the overestimated $\Sigma_\mathrm{c}/\mathrm{D}^0$ baryon-to-meson ratio and the $\Lambda_\mathrm{c}^+(\leftarrow \Sigma_\mathrm{c}^{0,++}) \times 3/2$ / Λ_c^+ baryon-to-baryon ratio. The increase in the joinC parameter hints towards a larger production rate of excited spin-3/2 baryons that favorably decay to Λ_c instead of $\Sigma_\mathrm{c}(2455)$ baryons. In future research, joinC and the $\Sigma_\mathrm{c}(2455)$ spectra discussed in this thesis, can be further contrained when there are production measurements of these unobserved excited charmed baryon states, in particular, the $\Lambda_\mathrm{c}(2595), \Lambda_\mathrm{c}(2625)$ and $\Sigma_\mathrm{c}^{0,+,++}(2520)$ baryons [108]. Furthermore, this can also be extended to the b sector and the light-sector, as well as apply to multiple-heavy-flavored baryons.

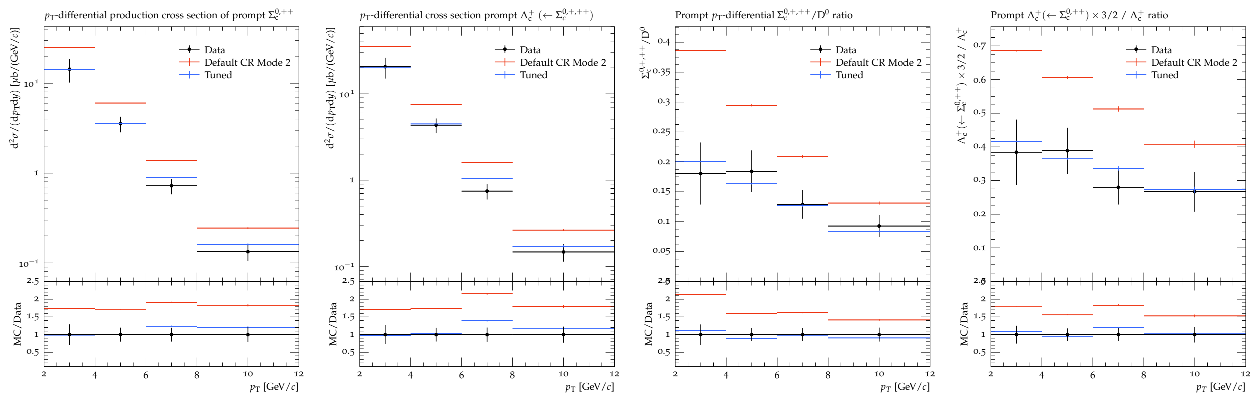

(a) (b) (c) (d)

Figure 32: Prompt (a) $\Sigma_c^{0,++}$ and (b) $\Lambda_c^+(\leftarrow \Sigma_c^{0,++}) \times 3/2$ p_T-differential cross sections. (c) $\Sigma_c^{0,+,++}/D^0$ and (d) $\Lambda_c^+(\leftarrow \Sigma_c^{0,++}) \times 3/2$ / Λ_c^+ ratios, compared with PYTHIA8 CR Mode 2 without (orange) and with our tuned values (blue).

Both mCv and joinC are close to the parameter guesses that were made in [58]. These tuned values can be used for future research on charm production in pp collisions with CR Mode 2. However, regarding all the changes in PYTHIA8.311, it would be wise to do a full retuning besides including these revisions.
The impact on Λ_c^+ and Ξ_c spectra with the tuned parameters is negligible, hence the Ξ_c spectra are still largely underestimated by the tuned QCD-CR Mode 2. We tested strangeness enhancement parameters (`StringFrag:strangeJunction`) for string breaks around a junction topology, which showed some increase in Ξ_c production but only a small amount. These parameters could be studied further, and potentially be tuned, to adequately predict Ξ_c production [58].

7 Conclusion and Outlook

In this thesis, the production of heavy-flavour hadrons in pp, p–Pb and Pb–Pb collisions are studied with various hadronisation models that are implemented in PYTHIA8, HERWIG7 and EPOS4. A selection of comparisons between simulated data and recent measurements by the ALICE experiment on meson-to-meson, baryon-to-meson and baryon-to-baryon production ratios were presented. It is observed that the default PYTHIA8 Monash tune and HERWIG7, both tuned on measurements in e^+e^- collisions, significantly underestimate charmed baryons production in pp collisions. On the other hand, both PYTHIA8 QCD-CR Mode 2 and Mode 0 describe Λ_c^+ production well due to the formation of string junctions and string fragmentation mechanisms. An increase in baryon production is also observed in the Baryonic Reconnection tune compared to the Plain Reconnection tune in HERWIG7 due to a larger baryonic cluster reconnection probability.

Furthermore, an increase in Λ_c^+ production is observed by adding beyond-leading-colour mechanisms in the hadronization of individual subcollisions in PYTHIA8 with Angantyr. This enhancement is seen without the assumption of QGP-like parton interactions. Therefore it would be interesting to study QGP-like interactions in heavy-ion collisions with EPOS4, by enabling the hydrodynamical evolution of the core, and compare this to experimental measurements and Angantyr.

In pp collisions, vector/pseudoscalar D-meson production ratios and $\Sigma_c(2455)$ baryon production are not well predicted by the PYTHIA8 QCD-CR Mode 2 tune. Therefore, a parameterization-based tuning was performed, utilizing the `Apprentice` framework, on the `StringFlav:mesonCvector` and `StringFlav:probQQ1toQQ0join` flavor selection parameters. The minimization of the goodness-of-fit measure was performed with the Truncated Newton method and a Bayesian inference technique. The resulting tuned parameters are given in Tab. 2. The predictions from PYTHIA8 with the tuned parameters are significantly improved for the D-meson ratios and Σ_c spectra, now describing the measurements within uncertainties.

In future research, `StringFlav:probQQ1toQQ0join` can be further studied by inspecting the productions of baryon species sensitive to spin-0 and spin-1 junction diquark formation, which would yield measurements of unobserved excited charmed baryon states. This research can also be continued in the b-sector and multiple-heavy-flavored baryons. Finally, the Ξ_c spectra are still largely underestimated by the tuned QCD-CR Mode 2. An additional strangeness enhancement mechanism is therefore needed to correctly describe strange heavy baryons with string models.

References

[1] A. Bazavov *et al.*, *"The equation of state in (2+1)-flavor QCD"*, Phys.Rev.D 90 (2014) 094503, `arXiv:1407.6387` [hep-lat], https://arxiv.org/abs/1407.6387.

[2] F. Halzen, A. Martin, *"Quarks and Leptons: An introductory course in Modern Particle Physics"*, Wiley, 1984.

[3] K. Nakamura *et al.*, *"Review of Particle Physics"*, J. Phys. G: Nucl. Part. Phys. 37 075021 (2010), DOI:10.1088/0954-3899/37/7A/075021.

[4] C. Patrignani *et al.*, *"Review of Particle Physics"*, Chin. Phys. C40, 100001 (2016), DOI: 10.1088/1674-1137/40/10/100001.

[5] R. L. Workman *et al.*, for the Particle Data Group Collaboration, *"Review of Particle Physics"*, PTEP, vol. 2022, p. 083C01 (2022), DOI: 10.1093/ptep/ptac097.

[6] L. Debbio, A. Ramos, *"Lattice determinations of the strong coupling"*, 2021. `arXiv:2101.04762` [hep-lat], https://arxiv.org/abs/2101.04762.

[7] B. Müller, *"Investigation of Hot QCD Matter: Theoretical Aspects"*, Phys. Scripta T 158 (2013) 014004, `arXiv:1309.7616` [nucl-th], https://arxiv.org/abs/1309.7616.

[8] ALICE Collaboration, *"Centrality determination in heavy ion collisions"*, ALICE-PUBLIC-2018-011 (2018).

[9] M.L. Miller, K. Reygers, S.J. Sanders and P. Steinberg, *"Glauber modeling in high energy nuclear collisions"*, Ann. Rev. Nucl. Part. Sci. 57 (2007) 205, `arXiv:0701025` [nucl-ex], https://arxiv.org/abs/nucl-ex/0701025.

[10] V.N. Gribov, *"Glauber corrections and the interaction between high-energy hadrons and nuclei"*, Sov. Phys. JETP 29 (1969) 483.

[11] M. Good, W. Walker, *"Diffraction disssociation of beam particles"*, Phys. Rev. 120 (1960) 1857.

[12] A. Silva, W.Serenone, D. Chinellato, J. Takahashi, C. Bierlich, *"Studies of heavy-ion collisions using PYTHIA Angantyr and UrQMD"*, `arXiv:2002.10236` [hep-ph], https://arxiv.org/abs/2002.10236.

[13] C. Bierlich, *"Multiparton Interactions and Underlying Event: a PYTHIA perspective"*, PoS HardProbes2020 (2021) 016.

[14] L. Lönnblad, H. Shahb, *"A spatially constrained QCD colour reconnection in pp, pA, and AA collisions in the PYTHIA8/Angantyr model"*, Eur.Phys.J.C 83 (2023) 7, 575, `arXiv:2303.11747` [hep-ph], https://arxiv.org/abs/2303.11747.

[15] C. Bierlich, G. Gustafson, L. Lönnblad, H. shah, *"The dynamic hadronization of charm quarks in heavy-ion collisions"*, Eur.Phys.J.C 84 (2024) 3, 231, `arXiv:2309.12452` [hep-ph], https://arxiv.org/abs/2309.12452.

[16] B. Andersson, G. Gustafson, B. Nilsson-Almqvist, *"A Model for Low p(t) Hadronic Reactions, with Generalizations to Hadron - Nucleus and Nucleus-Nucleus Collisions"*, Nucl. Phys. B 281 (1987) 289.

[17] H. Pi, *"An Event generator for interactions between hadrons and nuclei: FRITIOF version 7.0"*, Comput. Phys. Commun. 71 (1992) 173.

[18] A. Bialas, M. Bleszynski, W. Czyz, *"Multiplicity Distributions in Nucleus-Nucleus Collisions at High-Energies"*, Nucl. Phys. B 111 (1976) 461. 1.

[19] A. Festanti, *"Measurement of the D^0 meson production in Pb—Pb and p-–Pb collisions with the ALICE experiment at the LHC"*, Ph.D. dissertation, 2016 http://cds.cern.ch/record/2057663.

[20] M. Ploskon, *"Heavy-ion collisions - hot QCD in a lab"*, 2018, `arXiv: 1808.01411` [hep-ex], https://arxiv.org/abs/1808.01411.

[21] Particle Data Group, *"Review of Particle Physics"*, PTEP 2020 (2020) 8, 083C01.

[22] M. E. Peskin and D. V. Schroeder, *"An Introduction to Quantum Field Theory"*, Westview Press, 1995.

[23] M. L. Mangano, *"Two lectures on heavy quark production in hadronic collisions"*, Proc. Int. Sch. Phys. Fermi, vol. 137, pp. 95–137, 1998. `arXiv:9711337` [hep-ph], https://arxiv.org/abs/hep-ph/9711337.

[24] M. Giacalone, *"Study of charm hadronisation in pp collisions at $\sqrt{s} = 13$ TeV with the ALICE experiment"*, Ph.D. dissertation, 2023.

[25] S. Tang, *"Measurements of muons from open heavy-flavour hadron decays and jet particles in p–Pb and Pb–Pb collisions with ALICE at the LHC"*, Ph.D. dissertation, 2022.

[26] L. Vermont, *"Hadronisation of Heavy Quarks; production measurements of heavy-flavour hadrons from small to large collision systems"*, Ph.D. dissertation, 2022.

[27] S. López, *"Strange particle production in $t\bar{t}$ final states in pp collisions at $\sqrt{s} = 7$ TeV with the ATLAS detector at the LHC"*, Ph.D. dissertation, 2019.

[28] M. Jafarpour, *"Dynamical Thermalization in Heavy Ion Collisions"*, Ph.D. dissertation, 2022.

[29] M. Cacciari *et al.*, *"Theoretical predictions for charm and bottom production at the LHC"*, JHEP, vol. 10, p. 137, 2012. `arXiv:1205.6344` [hep-ph], https://arxiv.org/abs/1205.6344.

[30] I. Helenius, H. Paukkunen, *"Revisiting the D-meson hadroproduction in general-mass variable flavour number scheme"*, JHEP, vol. 05, p. 196, 2018, `arXiv:1804.03557` [hep-ph], https://arxiv.org/abs/1804.03557.

[31] ALICE Collaboration, S. Acharya *et al.*, *"Measurement of D^0, D^+, D^{*+} and D_s^+ production in pp collisions at $\sqrt{s} = 5.02$ TeV with ALICE"*, arXiv:1901.07979 [nucl-ex], https://arxiv.org/abs/1901.07979.

[32] ALICE Collaboration, S. Acharya *et al.*, *"D-meson production in p-Pb collisions at $\sqrt{s_{\rm NN}} = 5.02$ TeV and in pp collisions at $\sqrt{s} = 7$ TeV"*, Phys.Rev.C 94 (2016) 054908, 2016, arXiv:1605.07569 [nucl-ex], https://arxiv.org/abs/1605.07569.

[33] ALICE Collaboration, S. Acharya *et al.*, *"Measurement of beauty and charm production in pp collisions at $\sqrt{s} = 5.02$ TeV via non-prompt and prompt D mesons"*, JHEP, vol. 05, p. 220, 2021, arXiv:2102.13601 [nucl-ex], https://arxiv.org/abs/2102.13601.

[34] L. Gladilin, *"Fragmentation fractions of c and b quarks into charmed hadrons at LEP"*, Eur. Phys. J. C, vol. 75, no. 1, p. 19, 2015, arXiv:1404.3888 [hep-ex], https://arxiv.org/abs/1404.3888.

[35] ALICE Collaboration, S. Acharya *et al.*, *"Prompt D^0, D^+ and D^{*+} production in Pb–Pb collisions at $\sqrt{s_{\rm NN}} = 5.02$ TeV"*, JHEP 01 (2022) 174, arXiv:2110.09420 [nucl-ex], https://arxiv.org/abs/2110.09420.

[36] ALICE Collaboration, S. Acharya *et al.*, *"Measurement of beauty production via non-prompt D^0 mesons in Pb–Pb at $\sqrt{s_{\rm NN}} = 5.02$ TeV"*, JHEP 12 (2022) 126, 2022. arXiv:2202.00815 [nucl-ex], https://arxiv.org/abs/2202.00815.

[37] ALICE Collaboration, S. Acharya *et al.*, *"Charm production and fragmentation fractions at midrapidity in pp collisions at $\sqrt{s} = 13$ TeV"*, JHEP 12 (2023) 086, arXiv:2308.04877, https://arxiv.org/abs/2308.04877.

[38] ALICE Collaboration, S. Acharya *et al.*, *"Λ_c^+ production in pp and p–Pb collisions at $\sqrt{s_{\rm NN}} = 5.02$ TeV"*, Phys.Rev.C 104 (2021) 5, 054905, arXiv: 2011.06079, https://arxiv.org/abs/2011.06079.

[39] ALICE Collaboration, S. Acharya *et al.*, *"First measurement of Λ_c^+ down to $p_{\rm T} = 0$ in pp and p–Pb collisions at $\sqrt{s_{\rm NN}} = 5.02$ TeV"*, Phys.Rev.C 107 (2023) 6, 064901, arXiv:2211.14032 [nucl-ex], https://arxiv.org/abs/2211.14032.

[40] ALICE Collaboration, S. Acharya *et al.*, *"Measurement of prompt D^0, Λ_c^+, and $\Sigma_c^{0,+,++}(2455)$ production in pp collisions at $\sqrt{s} = 13$ TeV"*, Phys. Rev. Lett. (2022) 128, 012001, arXiv:2106.08278 [hep-ex], https://arxiv.org/abs/2106.08278.

[41] ALICE Collaboration, S. Acharya *et al.*, *"Measurement of the cross sections of Ξ_c^0 and Ξ_c^+ baryons and branching-fraction ratio $BR(\Xi_c^0 \to \Xi^- e^+ \nu_e)/\ BR(\Xi_c^0 \to \Xi^- \pi^+)$ in pp collisions at 13 TeV"*, Phys.Rev.Lett. 127 (2021) 27, 272001 arXiv:2105.05187 [nucl-ex], https://arxiv.org/abs/2105.05187.

[42] ALICE Collaboration, S. Acharya *et al.*, *"Λ_c^+ production in pp collisions at $\sqrt{s} = 7$ TeV and in p–Pb collisions at $\sqrt{s_{\rm NN}} = 5.02$ TeV"*, JHEP 04 (2018) 108, arXiv:1712.09581 [nucl-ex], https://arxiv.org/abs/1712.09581.

[43] ALICE Collaboration, S. Acharya *et al.*, *"Λ_c^+ production in pp collisions and in p–Pb collisions at $\sqrt{s_{NN}} = 5.02$ TeV"*, Phys.Rev.C 104 (2021) 5, 054905, arXiv:2011.06079 [nucl-ex], https://arxiv.org/abs/2011.06079.

[44] ALICE Collaboration, S. Acharya *et al.*, *"Constraining hadronization mechanisms with Λ_c^+/D^0 production ratios in Pb–Pb collisions at $\sqrt{s_{NN}} = 5.02$ TeV"*, Phys.Lett.B 839 (2023) 137796, arXiv:2112.08156 [nucl-ex], https://arxiv.org/abs/2112.08156.

[45] M. Arneodo, *"Nuclear effects in structure functions"*, Phys. Rep. 240 (1992) 301–393. 152 p. https://cds.cern.ch/record/238916.

[46] K. Eskola, P. Paakkinen, H. Paukkunen, and C. Salgado, *"Epps16: nuclear parton distributions with LHC data"*, Eur.Phys.J.C 77 (2017) 3, 163, arXiv:1612.05741 [hep-ph], https://arxiv.org/abs/1612.05741.

[47] R. Baier, A. Kovner, U. Wiedemann, *"Saturation and parton level Cronin effect: enhancement vs suppression of gluon production in p-A and A-A collisions"*, Phys.Rev.D 68 (2003) 054009, arXiv: 0305265 [hep-ph], https://arxiv.org/abs/hep-ph/0305265.

[48] S. Cao, G.-Y. Qin, and S. A. Bass, *Heavy-quark dynamics and hadronization in ultrarelativistic heavy-ion collisions: Collisional versus radiative energy loss*, Phys. Rev. C 88 (2013) 044907. arXiv:1308.0617 [nucl-th], https://arxiv.org/abs/1308.0617.

[49] R. Baier, Y. L. Dokshitzer, A. H. Mueller, S. Peigne, D. Schiff, *"Radiative energy loss and pT broadening of high-energy partons in nuclei"*, Nucl.Phys.B 484 (1997) 265-282, arXiv:hep-ph/9608322 [hep-ph], https://arxiv.org/abs/hep-ph/9608322.

[50] A. Schaelicke *et al.*, *"Event generator for particle production in high-energy collisions"*, Prog. Part. Nucl. Phys. 53 (2004) 329–338, arXiv:hep-ph/0311270 [hep-ph], https://arxiv.org/abs/hep-ph/0311270.

[51] ATLAS Collaboration, *"Measurement of underlying event characteristics using charged particles in pp collisions at $\sqrt{s} = 900$ GeV and 7 TeV with the ATLAS detector"*, Phys. Rev. D 83 (2011) 112001, arXiv:1012.0791 [hep-ex], https://arxiv.org/abs/1012.0791.

[52] V. Sudakov, *"Vertex parts at very high-energies in quantum electrodynamics"*, Sov.Phys.JETP 3 (1956) 65-71, Zh.Eksp.Teor.Fiz. 30 (1956) 87-95.

[53] C. Bierlich *et al.*, *"A comprehensive guide to the physics and usage of PYTHIA 8.3"*, SciPost Phys.Codeb. 2022 (2022) 8, arXiv:2203.11601 [hep-ph], https://arxiv.org/abs/2203.11601.

[54] B. Andersson, G. Gustafson, G. Ingelman, T. Sjöstrand, *"Parton fragmentation and string dynamics"*, Phys.Rept. 97 (1983) 31-145.

[55] P. Edén, G.Gustafson, *"Baryon Production in the String Fragmentation Picture"*, Z.Phys.C 75 (1997) 41-49, arXiv:hep-ph/9606454 [hep-ph], https://arxiv.org/abs/hep-ph/9606454.

[56] B. Andersson, G. Gustafson, B. Söderberg, *"A probability measure on parton and string states"*, Nuclear Physics B 264 (1986), pp. 29–59, DOI: 10.1016/0550-3213(86)90471-2.

[57] J. Christiansen, P. Skands, *"String Formation Beyond Leading Colour"*, JHEP 08 (2015) 003, arXiv:1505.01681 [hep-ph], https://arxiv.org/abs/arXiv:1505.01681.

[58] J. Altmann, P. Skands, *"String Junctions Revisited"*, arXiv:2404.12040v1 [hep-ph], https://arxiv.org/abs/2404.12040.

[59] C. Bierlich, G. Gustafson, L. Lönnblad, H. Shah, *"The Angantyr model for Heavy-Ion Collisions in PYTHIA8"*, JHEP 10 (2018) 134, arXiv:1806.10820 [hep-ph], https://arxiv.org/abs/1806.10820.

[60] J. Bellm *et al.*, *"Herwig 7.0/Herwig++ 3.0 release note"*, Eur.Phys.J.C 76 (2016) 4, 196, arXiv:1512.01178 [hep-ph], https://arxiv.org/abs/1512.01178.

[61] S. Gieseke, P. Stephens, B. Webber, *"New formalism for QCD parton showers"*, JHEP 12 (2003) 045, arXiv:hep-ph/0310083 [hep-ph], https://arxiv.org/abs/hep-ph/0310083.

[62] M. Bahr *et al.*, *"Herwig++ Physics and Manual"*, Eur.Phys.J.C 58 (2008) 639-707, arXiv:0803.0883 [hep-ph], https://arxiv.org/abs/0803.0883.

[63] A. Kupco, *"Cluster hadronization in HERWIG 5.9"*, Workshop on Monte Carlo Generators for HERA Physics (Plenary Starting Meeting), pp. 292–300, 1998, arXiv:hep-ph/9906412 [hep-ph], https://arxiv.org/abs/hep-ph/9906412.

[64] S. Gieseke, C. Rohr, A. Siodmok, *"Colour reconnections in Herwig++"*, Eur.Phys.J.C 72 (2012) 2225, arXiv:1206.0041 [hep-ph], https://arxiv.org/abs/1206.0041.

[65] D. Reichelt, P. Richardson, A. Siodmok, *"Improving the Simulation of Quark and Gluon Jets with Herwig 7"*, Eur.Phys.J.C 77 (2017) 12, 876, arXiv:1708.01491 [hep-ph], https://arxiv.org/abs/1708.01491.

[66] S. Gieseke, P. Kirchgaeßer, S. Plätzer, *"Baryon production from cluster hadronisation"*, Eur.Phys.J.C 78 (2018) 2, 99, arXiv:1710.10906 [hep-ph], https://arxiv.org/abs/1710.10906.

[67] M. Bahr, S. Gieseke, M. Seymour, *"Simulation of multiple partonic interactions in Herwig++"*, JHEP 07 (2008) 076, arXiv:0803.3633 [hep-ph], https://arxiv.org/abs/0803.3633.

[68] H. Drescher, M. Hladik, S. Ostapchenko, T. Pierog, K. Werner, *"Parton-based Gribov–Regge theory"*, Phys.Rept. 350 (2001) 93-289, arXiv:hep-ph/0007198 [hep-ph], https://arxiv.org/abs/hep-ph/0007198.

[69] J. Jahan, *"The Beam Energy Scan under the scope of EPOS 4: Studying the impact of hadronic cascades on the 2nd order cumulants of conserved net-charges in heavy-ion collisions"*, Ph.D. dissertation, Nantes Université, 2022.

[70] K. Werner, *"Gribov-Regge approach and EPOS"*, Lecture, given in KSETA Topical courses. Germany, 2019, https://hal.archives-ouvertes.fr/hal-02434245.

[71] X. Artru and G. Mennessier, *"String model and multiproduction"*, Prog.Theor.Phys. 61 (1979) 218, doi: 10.1016/0550-3213(74)90360-5.

[72] K. Werner, *"Revealing a deep connection between factorization and saturation: New insight into modeling high-energy proton-proton and nucleus-nucleus scattering in the EPOS4 framework"*, Phys.Rev.C 108 (2023) 6, 064903, arXiv:2301.12517 [hep-ph], https://arxiv.org/abs/2301.12517.

[73] L. McLerran, R. Venugopalan, *"Gluon Distribution Functions for Very Large Nuclei at Small Transverse Momentum"*, Phys.Rev.D 49 (1994) 3352-3355, arXiv:hep-ph/9311205 [hep-ph], https://arxiv.org/abs/hep-ph/9311205.

[74] K. Werner, *"Core-corona procedure and microcanonical hadronization to understand strangeness enhancement in proton-proton and heavy ion collisions in the EPOS4 framework"*, Phys.Rev.C 109 (2024) 1, 014910, arXiv:2306.10277 [hep-ph], https://arxiv.org/abs/2306.10277.

[75] K. Werner, *"Core-Corona Separation in Ultra-Relativistic Heavy Ion Collisions"*, Phys.Rev.Lett. 98 (2007) 152301, arXiv:0704.1270 [nucl-th], https://arxiv.org/abs/0704.1270.

[76] K. Werner *et al.*, *"Analyzing radial flow features in p–Pb and p–p collisions at several TeV by studying identified-particle production with the event generator EPOS3"*, Phys.Rev.C 89 (2014) 6, 064903, arXiv:1312.1233 [nucl-th], https://arxiv.org/abs/1312.1233.

[77] K. Werner, F. Liu, T. Pierog, *"Parton Ladder Splitting and the Rapidity Dependence of Transverse Momentum Spectra in Deuteron-Gold Collisions at RHIC"*, Phys.Rev.C 74 (2006) 044902, arXiv:0506232 [hep-ph], https://arxiv.org/abs/hep-ph/0506232.

[78] K. Werner, B. Guiot, *"Perturbative QCD concerning light and heavy flavor in the EPOS4 framework"*, Phys.Rev.C 108 (2023) 3, 034904, arXiv:2306.02396 [hep-ph], https://arxiv.org/abs/2306.02396.

[79] M. Stefaniak, K. Werner, H.P. Zbroszczyk, J. Jahan, *"Equation of state within the EPOS3 model"*, Phys.Rev.C 108 (2023) 1, 014905, arXiv:2209.12979 [hep-ph], https://arxiv.org/abs/2209.12979.

[80] J. Zhao, J. Aichelin, P. Gossiaux, V.Ozvenchuk, K.Werner *"Heavy flavour hadron production in relativistic heavy ion collisions at RHIC and LHC in EPOS4HQ"*, 2024, arXiv:2401.17096 [hep-ph], https://arxiv.org/abs/2401.17096.

[81] J.Zhao, J. Aichelin, P. Gossiaux, K. Werner, *"Heavy flavor as a probe of hot QCD matter produced in proton-proton collisions"*, Phys.Rev.D 109 (2024) 5, 054011, arXiv:2310.08684 [hep-ph], https://arxiv.org/abs/2310.08684.

[82] M. Bleicher *et al.*, *"Relativistic hadron hadron collisions in the ultrarelativistic quantum molecular dynamics model"*, J.Phys.G 25 (1999) 1859-1896, `arXiv:hep-ph/9909407` [hep-ph], https://arxiv.org/abs/hep-ph/9909407.

[83] H. Petersen *et al.*, *"Fully integrated transport approach to heavy ion reactions with an intermediate hydrodynamic stage"*, Phys.Rev.C 78 (2008) 044901, `arXiv:0806.1695` [nucl-th], https://arxiv.org/abs/0806.1695.

[84] F. Close, *"An Introduction to Quarks and Partons"*, Academic Press, Inc; New York, NY; ISBN 0-12-175150-3.

[85] C. Bierlich *et al.*, *"Robust Independent Validation of Experiment and Theory: Rivet version 3"*, SciPost Phys. 8 (2020) 026, `arXiv: 1912.05451` [hep-ph], https://arxiv.org/abs/1912.05451.

[86] C. Bierlich *et al.*, *"Confronting experimental data with heavy-ion models: RIVET for heavy ions"*, Eur.Phys.J.C 80 (2020) 5, 485, `arXiv:2001.10737` [hep-ph], https://arxiv.org/abs/2001.10737.

[87] P. Skands, S. Carrazza, J. Rojo, *"Tuning PYTHIA 8.1: the Monash 2013 Tune"*, Eur.Phys.J.C 74 (2014) 8, 3024, `arXiv:1404.5630` [hep-ph], https://arxiv.org/abs/1404.5630.

[88] ALICE Collaboration, J. Adam *et al.*, *"Measurement of pion, kaon and proton production in proton–proton collisions at $\sqrt{s} = 7$ TeV"*, Eur.Phys.J.C 75 (2015) 5, 226, `arXiv:1504.00024` [nucl-ex], https://arxiv.org/abs/1504.00024.

[89] B. Nejad, W. Kilian, J. M. Lindert, S. Pozzorini, J. Reuter, C. Weiss, *"NLO QCD predictions for off-shell $t\bar{t}$ and $t\bar{t}H$ production and decay at a linear collider"*, JHEP 12 (2016) 075, `arXiv:1609.03390` [hep-ph], https://arxiv.org/abs/1609.03390.

[90] *"Rivet webpage"*, https://rivet.hepforge.org/analyses.html.

[91] A. Silva, *"Rivet and the analysis preservation in heavy-ion collisions experiments"*, Rev.Mex.Fis.Suppl. 3 (2022) 4, 040909, `arXiv:2301.02704` [nucl-ex], https://arxiv.org/abs/2301.02704.

[92] M. Gutiérrez A., F. Vexo, D. Thalmann, *"Stepping into Virtual Reality"*, Springer London, 2008.

[93] ALICE Collaboration, *"Performance of the ALICE VZERO system"*, JINST 8 (2013) P10016, `arXiv:1306.3130` [nucl-ex], https://arxiv.org/abs/1306.3130.

[94] M. Dobbs and J. B. Hansen, *"The HepMC C++ Monte Carlo event record for High Energy Physics"*, Computer Physics Communications 134 no. 1, (2001) 41–46.

[95] *"PYTHIA8 webpage"*, https://pythia.org/.

[96] *"PYTHIA Soft QCD Settings"*, https://pythia.org//latest-manual/QCDSoftProcesses.html.

[97] M. Rybczynski, G. Stefanek, W. Broniowski, P. Bozek, *"GLISSANDO 2: GLauber Initial-State Simulation AND mOre..., ver. 2*"*, Comput.Phys.Commun. 185 (2014) 1759-1772, `arXiv:1310.5475` [nucl-th], https://arxiv.org/abs/1310.5475.

[98] *"HERWIG7 webpage"*, https://herwig.hepforge.org/.

[99] *"HERWIG7: Minimum-bias and underlying-event tunes"*, https://herwig.hepforge.org/tutorials/mpi/tunes.html.

[100] *"EPOS4 webpage"*, https://klaus.pages.in2p3.fr/epos4/.

[101] C. Bierlich, *"Hadronisation Models and Colour Reconnection"*, PoS DIS2016 (2016) 051, `arXiv:1606.09456` [hep-ph], https://arxiv.org/abs/1606.09456.

[102] C. Bierlich, *"Rope Hadronization and Strange Particle Production"*, EPJ Web Conf. 171 (2018) 14003, `arXiv:1710.04464` [nucl-th], https://arxiv.org/abs/1710.04464.

[103] M. Krishnamoorthy, H. Schulz, X. Ju, W. Wang, S. Leyffer, Z. Marshall, S. Mrenna, J. Muller, J. B. Kowalkowski, *"Apprentice for Event Generator Tuning"*, EPJ Web Conf. 251 (2021) 03060, `arXiv:2103.05748` [hep-ex], https://arxiv.org/abs/2103.05748.

[104] M. Fieg, F. Kling, H. Schulz, T.Sjöstrand, *"Tuning Pythia for Forward Physics Experiments"*, Phys.Rev.D 109 (2024) 1, 016010, `arXiv:2309.08604` [hep-ph], https://arxiv.org/abs/2309.08604.

[105] A. Buckley, H.Hoeth, H. Lacker, H. Schulz, J. von Seggern, *"Systematic event generator tuning for the LHC"*, Eur.Phys.J.C 65 (2010) 331-357, `arXiv:0907.2973` [hep-ph], https://arxiv.org/abs/0907.2973.

[106] R. Rembo. T. Steihaug, *"Truncated-Newton algorithms for large-scale unconstrained optimization"*, Mathematical Programming. (1983) 26 (2). Springer: 190–212.

[107] F. Feroz, M.P. Hobson, M. Bridges, *"MultiNest: an efficient and robust Bayesian inference tool for cosmology and particle physics"*, Mon.Not.Roy.Astron.Soc. 398 (2009) 1601-1614, `arXiv:0809.3437` [astro-ph], https://arxiv.org/abs/0809.3437.

[108] J. Altmann, A. Dubla, V. Greco, A. Rossi, P. Skands *"Towards the understanding of heavy quarks hadronization: from leptonic to heavy-ion collisions"*, `arXiv:2405.19137` [hep-ph], https://arxiv.org/abs/2405.19137.

A Appendix A

A.1 Complementary figures pp collisions

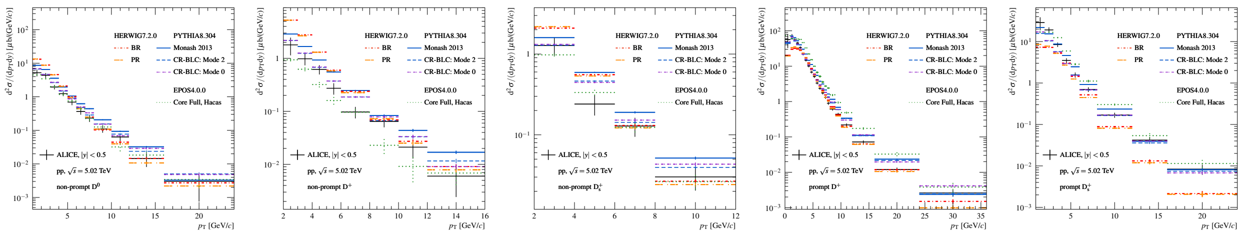

(a) (b) (c) (d) (e)

Figure 33: The p_{T}-differential production cross section at midrapidity of non-prompt (a) D^0, (b) D^+, (c) $\mathrm{D}_{\mathrm{s}}^+$ and prompt (d) D^+ and (e) $\mathrm{D}_{\mathrm{s}}^+$ mesons in pp collisions at $\sqrt{s} = 5.02$ TeV measured by the ALICE experiment [33], compared with different MC generators.

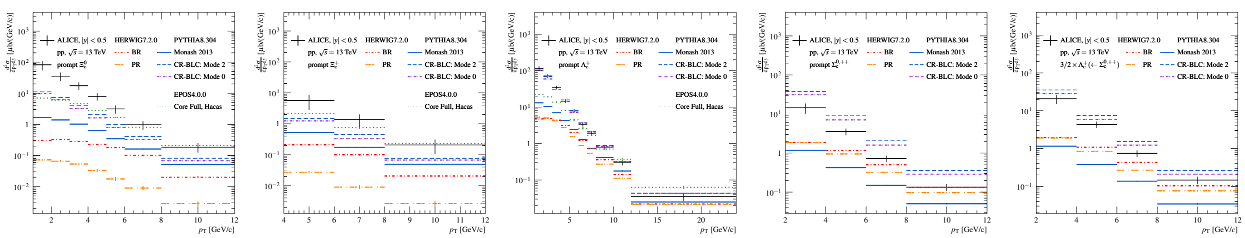

(a) (b) (c) (d) (e)

Figure 34: The p_{T}-differential production cross section at midrapidity of prompt (a) Ξ_{c}^0, (b) Ξ_{c}^+, (c) Λ_{c}^+, (d) $\Sigma_{\mathrm{c}}^{0,++}$ and (e) $\Lambda_{\mathrm{c}}^+(\leftarrow \Sigma_{\mathrm{c}}^{0,++})$ baryons in pp collisions at $\sqrt{s} = 13$ TeV measured by the ALICE experiment [37, 40], compared with different MC generators.

A.2 Complementary figures heavy-ion collisions

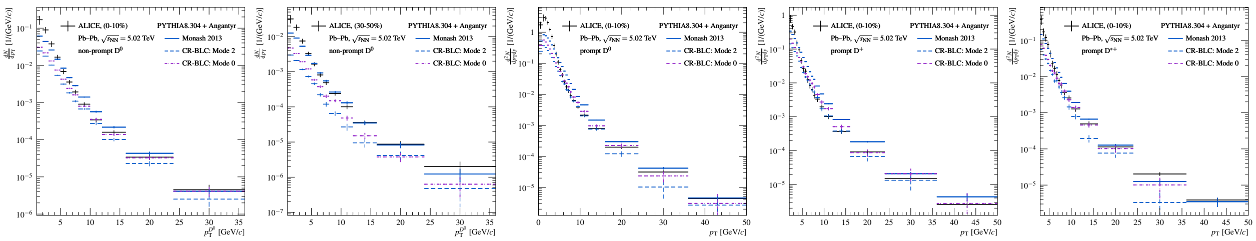

(a) (b) (c) (d) (e)

Figure 35: The p_{T}-differential production yield in Pb–Pb collisions of non-prompt (a) D^0 for 0-10% and (b) D^0 at 30-50% centrality bin. Production yield in Pb–Pb collisions for 0-10% centrality bin of prompt (c) D^0, (d) D^+ and (e) D^{*+} mesons at $\sqrt{s} = 5.02$ TeV measured by the ALICE experiment [35, 36], compared with different PYTHIA8 models.